The origin of fluorite-barite mineralization at the interface between the Paris Basin and its Variscan basement: insights from fluid inclusion chemistry and isotopic (O, H, Cl) composition

Louise Lenoir, Thomas Blaise, Diana Chourio-Camacho, Antonin Richard, Alexandre Tarantola, Pierre Agrinier, Thomas Rigaudier, Gaël Monvoisin, Gérard Bardoux, Benjamin Brigaud, et al.

The origin of fluorite-barite mineralization at the interface between the Paris Basin and its Variscan basement: Insights from fluid inclusion chemistry and isotopic (O, H, Cl) composition

Mineralium Deposita

Authors:

Louise Lenoir[1*] (0000-0003-0954-2714)

Thomas Blaise[1] (0000-0003-1820-8152)

Diana Chourio-Camacho[2] (0000-0001-7094-9041)

Antonin Richard[3] (0000-0002-0702-4764)

Alexandre Tarantola[3] (0000-0002-5145-2344)

Pierre Agrinier[4] (0000-0002-5119-2423)

Thomas Rigaudier[5] (0000-0003-4947-3784)

Gaël Monvoisin[1] (0000-0001-9947-342X)

Gérard Bardoux[4] (0000-0002-7398-1415)

Benjamin Brigaud[1] (0000-0001-6961-2177)

Jocelyn Barbarand[1] (0000-0003-2166-9232)

[1]Université Paris-Saclay, CNRS, GEOPS, 91405, Orsay, France

[2]Université PSL, MINES ParisTech, Centre de Géosciences, 77300, Fontainebleau, France

[3]Université de Lorraine, CNRS, GeoRessources Laboratory, B.P. 70239, F-54506 Vandœuvre-lès-Nancy, France

[4] Université Paris Cité, Institut de physique du globe de Paris, CNRS, 75005 Paris, France

[5]Université de Lorraine, Centre de Recherche Pétrographiques et Géochimiques, UMR 7358 CNRS, France

*Correspondence to: Louise Lenoir (louise.lenoir2@gmail.com)

Abstract

We provide new constraints for the fluid flow system at the origin of two F-Ba deposits located at the unconformity between the south of the Paris Basin and the northern edge of the French Massif Central. We used microthermometry and bulk crush-leach analyses to determine isotope ratios of mineralizing fluids ($\delta^{18}O$, δD, $\delta^{37}Cl$), together with cation and anion composition of fluid inclusions hosted by fluorite. Chlorinity and Cl/Br molar ratios (212-521) indicate the involvement of a brine, whose origin likely corresponds to Triassic evaporated seawater compatible with supratidal dolomitic facies preserved nearby. Microthermometry reveals high Ca/Na ratios, suggesting that the brine composition evolved from hydrothermal alteration of the Variscan basement and partial dissolution and replacement of the host sedimentary rocks. $\delta^{37}Cl$ values are lower than the expected value of evaporated seawater, suggesting Cl isotope fractionation by ion filtration in clay-rich horizons. Fluorite crystallized at minimum temperatures of 70 to 110 °C, 10-40 °C warmer than the host Triassic sedimentary rocks. Ascending brines were expelled during the Early Cretaceous and experienced a drop in pressure and temperature, together with possible mixing with the SO_4-rich pore water of the sedimentary rocks, causing precipitation of silica, followed by fluorite and barite, forming a stratabound deposit similar to those found in many areas in Western Europe.

Keywords: F-Ba deposit, fluid inclusion**,** chlorine isotope**,** granite hydrothermal alteration**,** Paris Basin

Introduction

In Western Europe, the unconformity between the Variscan crystalline basement and the Mesozoic sedimentary cover hosts a large diversity of deposits of economically attractive elements such as U, Pb, Zn, Cu, Au, Bi, F and Ba (Banks et al. 2002; Sanchez et al. 2009; Haschke et al. 2021). Fluorite-barite mineralization may occur as veins in the basement (Cardellach et al. 1990; Galindo et al. 1994; Munoz et al. 1999; Fourcade et al. 2002; Baatartsogt et al. 2007;

De Graaf et al. 2019; Walter et al. 2018) as well as replacing Mesozoic sedimentary rocks (Sizaret 2003; Boiron et al. 2010; Gigoux et al. 2016). Among these deposits, fluorite-barite mineralization is well developed on the southern border of the Paris Basin. World-class deposits hosted in Late Triassic rocks are known at the interface between the Paris Basin and the Variscan basement (Soulé de Lafont and Lhégu, 1980; Gigoux et al., 2016). Significant fluorite deposits are hosted as stratabound deposits in Late Triassic silicified sedimentary rocks lying unconformably over Paleozoic granitic rocks. A syn-sedimentary origin was first proposed (Boirat et al. 1980; Davaine 1980; Soulé de Lafont and Lhégu 1980). Nigon (1988) and Gigoux et al. (2016) documented minimal trapping temperatures of fluid inclusions in fluorite in the range 80-100 °C. Sm-Nd geochronology on fluorite (Gigoux et al. 2015) revealed that precipitation occurred during the Early Cretaceous period. Driving mechanisms for mineralization remain unclear, as well as the origin of heat, fluids and elements.

Gigoux et al. (2016) highlighted thermal disequilibrium between mineralizing fluids and the host sedimentary rocks of about 40 °C during deposition (Uriarte 1997). Similar hydrothermal activity has been documented in the central and eastern parts of the Paris Basin (Brigaud et al. 2020; Mangenot et al. 2017), recording fluid ascent along deeply rooted faults. Boiron et al. (2002), Cathelineau et al. (2012) and Gigoux et al. (2016) suggested that precipitation resulted from the mixing of diluted cool water with dense sedimentary brines percolating downwards through the crystalline basement. Mixing between ascending fluids and formation water has been documented in several F-Ba-Pb-Zn-Cu stratabound and vein deposits across Western Europe (e.g., Trinkler et al. 2005; Baatartsogt et al. 2007; Fusswinkel et al. 2013; De Graaf et al. 2019).

Different mechanisms have been proposed to explain the origin of mineralizing brines. Using Cl/Br and Na/K ratios in fluorite, quartz or dolomite fluid inclusions, De Graaf et al. (2019) showed evaporation of seawater (primary brine) in Central Germany, whereas Banks et al. (2000) and Cathelineau et al. (2012) proposed evaporite dissolution (secondary brine) in Colombia and Western France, respectively. In the Schwarzwald district, SW Germany, Walter et al. (2017) used Cl/Br ratios to show that Jurassic–Cretaceous veins formed by the mixing of primary and secondary brines displaying similar salinities. Interaction with basement rocks is also likely considered, meteoric water percolated to

depth of at least 10 km (Munoz et al. 1999; Gleeson et al. 2003; Diamond et al. 2018). In such conditions, mineral hydration reactions can consume H_2O and thus increase salinity of the interacting fluid (Stober and Bucher, 2004; Burisch et al. 2016). In addition, the low δD values of fluid inclusions in fluorite, in mineralization developed in the northeastern and southeastern borders of the French Massif Central (FMC), were attributed to fluids of meteoric origin (Munoz et al. 1999; Sizaret et al. 2004, 2009).

Cl/Br ratios and chlorine stable isotope compositions in fluid inclusions can efficiently discriminate fluid origins (e.g., Frape et al. 1984; Richard et al. 2011) but, such data is scarce in F-Ba stratabound and vein deposits from the borders of the FMC. The few data comes from Boiron et al. (2002) in the northwestern part of the FMC, where fluorite fluid inclusion high Cl content, together with Cl/Br ratios lower than the average seawater value, were interpreted as resulting from seawater evaporation during the Late Triassic to Early Jurassic (Boiron et al. 2002). Because multiple fluids can be involved in mineral deposition at the basement-cover unconformity (Walter et al. 2018), a detailed study of fluid inclusion physical-chemical characteristics is essential to provide robust genetic models (Burisch et al. 2017; Walter et al. 2018).

This study builds on the works of Gigoux et al. (2015, 2016) by characterizing the chemical and isotopic compositions of fluorite inclusion fluids coming from two massive stratabound F-Ba deposits in the south of the Paris Basin. We focus on the origin of dissolved chlorine through the measurements of major dissolved ions and $\delta^{18}O$, δD and $\delta^{37}Cl$ values in fluid inclusions using bulk crush-leach methods. Three fluorite generations were documented at Pierre-Perthuis (Gigoux et al. 2016; Lenoir et al. 2021). The first and last fluorite stages correspond to translucent to purple fluorite and were not considered for this research because the crystals are too small, sub millimetric in size, and devoid of fluid inclusions. Therefore, only the second fluorite stage dated at 130 ± 15 Ma by Sm-Nd geochronology is considered (Gigoux et al. 2016; Lenoir et al. 2021). This stage is represented by large yellow-honey fluorite crystals, well-developed in geodes and veins and thus allowing for sampling for analytical methods used in this study. Our main objectives are to identify the origin of mineralizing fluids and to clarify the sources of F, Ba, Si, S and the mechanisms of mass transfer and mineral precipitation, then compare the physical, chemical and isotopic characteristics of paleo-

fluids trapped in fluorite inclusions with present-day pore water in deep aquifers of the Paris Basin and Rhine graben above the Paleozoic basement. From this comparison, we further discuss fluid sources and mixing between the basement and deep sedimentary reservoirs.

Geological context

Mesozoic sedimentary rocks of the south-eastern part of the intracratonic Paris Basin overlie unconformably Paleozoic rocks outcropping in the Morvan Massif (Vialette 1973; Lardeaux et al. 2014) at the northern edge of the FMC. The massif is mainly composed of granitic, metamorphic and volcano-sedimentary units that formed during the Early and Late Carboniferous (Fig. 1, Vialette 1973; Lardeaux et al. 2014). The FMC is known to contain massive stratabound fluorite deposits, some of which are of economic grade (Fig. 1b): Egreuil (0.4 Mt CaF_2), Marigny-sur-Yonne (0.5 Mt CaF_2), Pontaubert (0.6 Mt CaF_2), Courcelles-Frémoy (1 Mt CaF_2), Pierre-Perthuis (1.4 Mt CaF_2) and Antully (1.6 Mt CaF_2, Soulé de Lafont and Lhégu, 1980). The two fluorite deposits studied are at the unconformity between the southern Paris Basin and the north-western part of the Morvan Massif (Fig. 1a). Both are hosted in the Carnian-Norian Assise de Chitry Formation, above the crystalline basement. This formation is heterogeneous, being karstified or brecciated and of variable thickness (Lefavrais- Raymond et al., 1965). The primary mineralogy of this formation is controversial as it is now largely silicified. It reveals ghosts of evaporite, algal and stromatolitic veils as well as desiccation cracks (Bois, 1978). It was originally calcareous, but was extensively dolomitized and later replaced by chalcedony, fluorite and barite (Gigoux et al. 2016) and hence hosts most of the fluorite and barite resources.

The Pierre-Perthuis deposit hosts the main fluorite resources in France, estimated at 1.4 million tonnes of CaF_2 (De Launay 1913; Soulé de Lafont and Lhégu 1980). Most of this resource is stratabound in the Assise de Chitry Formation. The Pierre-Perthuis fluorite deposit is near a regional N-S normal fault with an offset estimated at 100 m (Soulé de Lafont and Lhégu, 1980).

Situated 35 km southeast of Pierre-Perthuis near another N-S normal fault, the La Collancelle deposit consists of massive fluorite and barite crystals associated with minor sulfides (mainly galena and chalcopyrite) in the Assise de Chitry Formation above Paleozoic rhyolitic basement (Scolari 1966).

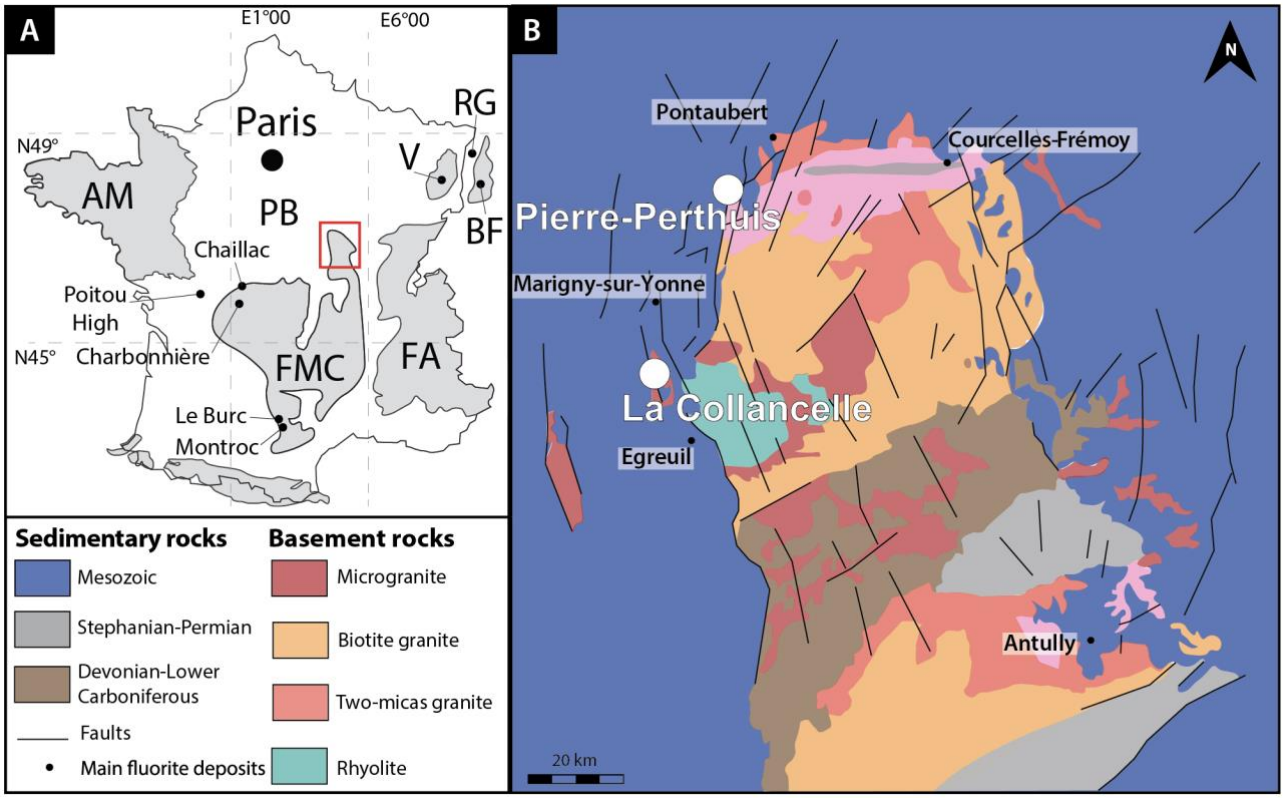

Fig. 1 a) Regional settings. b) Geological map of the Morvan massif with the location of the fluorite deposits from Pierre-Perthuis and La Collancelle (modified according the 1:1,000,000 geological map, French Geological Survey). AM : Armorican Massif, BF : Black Forest, FA : French Alps, FMC : French Massif Central, PB : Paris Basin, RG : Rhine Graben, V : Vosges Massif.

Material and methods

Sampling strategy and fluid inclusion petrography

Centimetric fluorite crystals from Pierre-Perthuis and La Collancelle were collected in outcrops. At Pierre-Perthuis, centimetric fluorite crystals filling cavities were sampled in three areas: (1) Bois Dampierre, (2) Bois de l'Epenay and (3) La Roche Percée (Fig. 2a), (Fig. 2c).

At La Collancelle, F-Ba mineralization forms large veins that were excavated during the construction of the Nivernais canal (Fig. 2b). These fluorite crystals are similar to the ones from Pierre-Perthuis, with zoning marked by growth stages of a milky aspect rich in fluid inclusions alternating with more translucent layers (Fig. 2d). The age of fluorite precipitation at La Collancelle is unknown. All samples are presented in electronic supplementary material (ESM1, Table S1).

Twenty polished thin sections (30 µm) were prepared and studied using optical and cathodoluminescence microscopy.

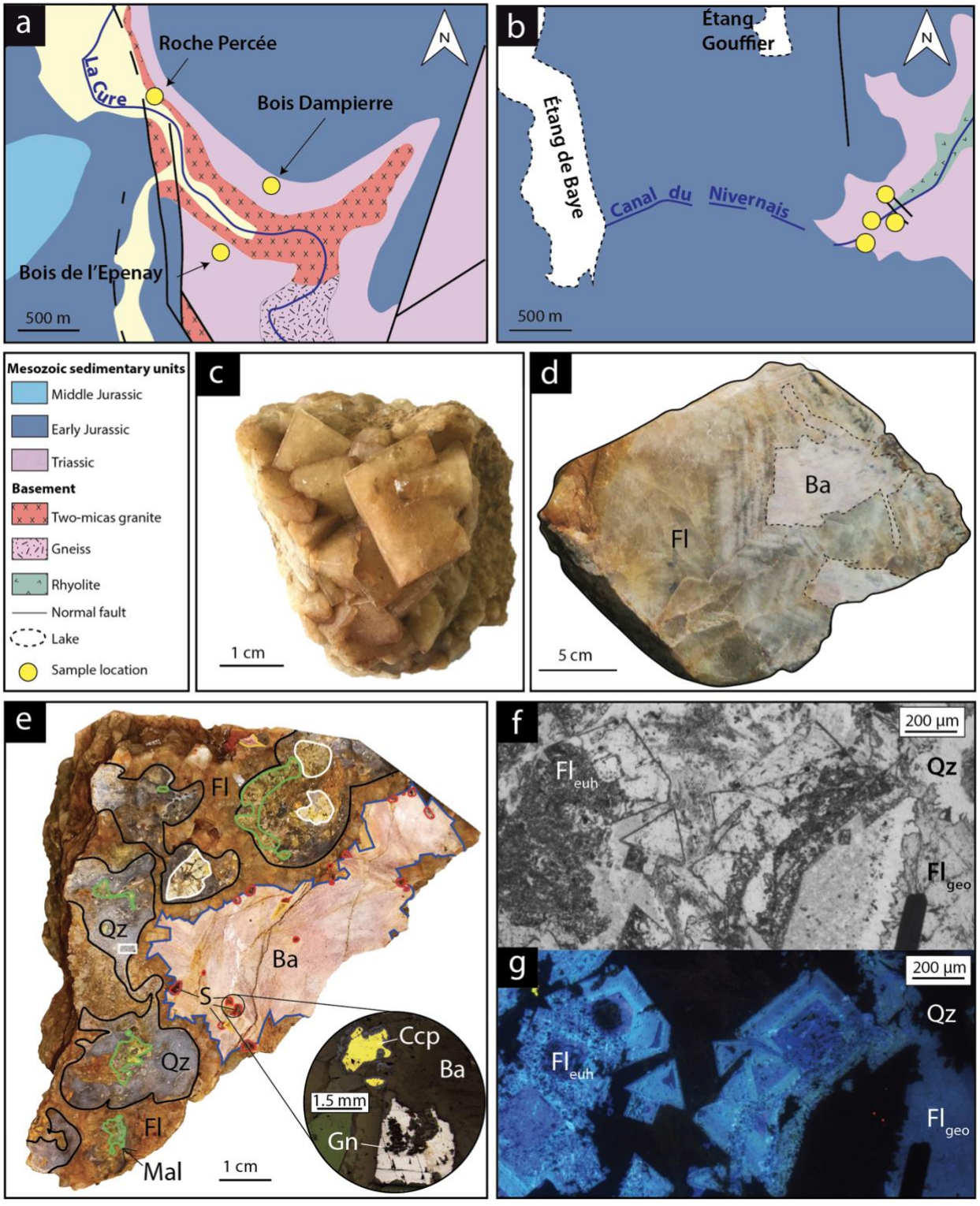
a
Roche Percée
La Cure
Bois Dampierre
Bois de l'Epenay
500 m
N
b
Étang Gouffier
Étang de Baye
Canal du Nivernais
500 m
N
Mesozoic sedimentary units
Middle Jurassic
Early Jurassic
Triassic
Basement
Two-micas granite
Gneiss
Rhyolite
Normal fault
Lake
Sample location
c
1 cm
d
Ba
Fl
5 cm
e
Fl
Qz
Ba
S
Qz
Fl
Mal
1 cm
Ccp
Ba
1.5 mm
Gn
f
200 µm
Fl euh
Qz
Fl geo
g
200 µm
Qz
Fl euh
Fl geo

Fig. 2 Location of the mineralized outcrops at (a) Pierre-Perthuis and (b) La Collancelle. (c) Geodic fluorite sample from Pierre-Perthuis (Gigoux 2016, sample PP16). (d) Fluorite-barite from La Collancelle. (e) Mineralized sample from Pierre-Perthuis. The silicified host rock (circled in black) contains clasts of the underlying altered granite (outlined in white). The circular inset is a microphotograph (reflected light) of Ccp and Gn crystals included in barite. Microphotographs in (f) plane polarized light and (g) cathodoluminescence microscopy illustrating two fluorite growth stages. Fl_{euh} is the first euhedral fluorite generation showing sector zoning, not investigated in this study. Fl_{geo} is the second fluorite generation, showing homogeneous and dull cathodoluminescence, corresponding to the geodic crystals illustrated in (c) and (e). Fl: fluorite; Ba: Barite; Qz: Quartz; Mal: Malachite; Ccp: Chalcopyrite; Gn: Galena

Fluid inclusion microthermometry

Microthermometry was carried out on 10 double-polished 200-µm-thick sections using a semi-automatic gas-flow heating-cooling Linkam MDS 600 stage attached to a Leica DM2500 optical microscope. The stage was calibrated using two synthetic standards (pure water FI with critical density, which homogenizes at 374 °C and an in-house three-phase H_2O-CO_2 FI with a melting temperature of CO_2 calibrated at –58.1 °C. Applied corrections are documented in ESM1 (Table S2). The composition of two-phase aqueous fluid inclusions (liquid and vapor) was approximated in the NaCl-$CaCl_2$-H_2O system because (1) three phase transitions were observed at low temperatures (Steele MacInnis et al. 2016) and (2) first ice melting temperature was measured from –54 to –46 °C (Yanatieva 1946). Total salinities (NaCl + $CaCl_2$) are expressed as 'Swt' in weight percent equivalent (wt.%) NaCl + $CaCl_2$, from the dissolution temperature of hydrohalite and the melting temperature of ice (Tm_{hh} and Tm_{ice}) using the Excel® spreadsheet of Steele-MacInnis et al. (2011). The first melting of a solid phase was difficult to observe and is given with a precision of ±2 °C, estimated from repeated measurements in the largest FI (Te*). The dissolution temperature of hydrohalite (Tm_{hh}) and melting temperature of ice (Tm_{ice}) are reported with an accuracy of 1 and 0.1 °C respectively, and homogenization temperature (Th) is ±1 °C. Each fluid inclusion was measured twice. Data that could not be replicated were discarded. The few

fluid inclusions belonging to the same assemblage having variable liquid-vapor ratios were excluded and considered to have been affected by post-trapping deformation (stretching, leakage) or necking-down (Goldstein and Reynolds 1994). In small fluid inclusions (< 10 µm), the melting temperature of antarcticite, hydrohalite and ice were not measured (Chu et al. 2016). A total of 171 fluid inclusions were observed and measured, 70 from Pierre-Perthuis and 101 from La Collancelle.

Fluid inclusion oxygen and hydrogen stable isotope composition

Oxygen and hydrogen stable isotope compositions were measured at the CRPG (Université de Lorraine - CNRS, Vandoeuvre-lès-Nancy, France) on eight samples from Pierre-Perthuis and eight samples from La Collancelle. Individual fluorite zones were extracted from the host rocks and reduced into pieces of 1 to 5 mm. Mineral impurities were removed manually under the binocular microscope. Each sample consists of 5 to 10 g of fluorite crystals. Samples were placed in stainless steel tubes and degassed overnight to remove adsorbed water at the crystal surfaces. Water trapped in fluid inclusions was extracted by mechanical crushing and vaporized by heating at a temperature of 250 °C. The liberated H_2O was collected in a liquid nitrogen cold trap at −170 °C and then separated from non-condensable gases. Water (70-285 µmol) was transferred to a micro-equilibration reactor into which 12 to 75 µmol CO_2 of known isotopic composition was added (ESM1, Table S3). Samples were placed at 25 °C for at least 24 h for a complete oxygen isotope equilibration between H_2O and CO_2. After this time, H_2O and CO_2 were separated cryogenically. The oxygen isotopic composition of equilibrated CO_2 was measured using a dual-inlet ThermoFisher MAT 253 mass spectrometer. The $\delta^{18}O$ of water was calculated using the mass balance equation of Kishima and Sakai (1980). After separation from CO_2 the water was reduced to H_2 using a uranium furnace heated to 800 °C for four Pierre-Perthuis samples. For the rest of the samples, the water was collected into a silica tube containing about 400 mg of fine-grained chromium and reduced into H_2 by Cr at 1,000 °C for 6 min. For all samples, H_2 was then transferred and quantified into a calibrated volume using a Toepler pump. All D/H ratios were measured using a dual-inlet GV

Isoprime mass spectrometer. Values are reported in per mil relative to the Vienna Standard Mean Ocean Water (V-SMOW) for oxygen and hydrogen. External reproducibility of the internal reference material was ± 2.0 ‰ and ± 0.5 ‰ for δD and $\delta^{18}O$ measurements respectively.

Major dissolved ions in fluid inclusions

Fluid inclusions were analyzed for their elemental composition using a bulk crush-leach method by mechanical crushing (Banks et al. 2000; Gleeson et al. 2003). For each sample, 1.5 to 50 g of fluorite crystals were separated from the host rocks. Mineral impurities were removed under the binocular tube. Crystals were washed twice using MilliQ water in an ultrasonic bath and then twice in boiling water for 10 min. Samples were then crushed in an agate mortar and inclusion fluids diluted by adding 10 to 12 mL of MilliQ water. After 12 hours of decantation, the electrolytic solutions were collected with single-use plastic syringes with a 0.2 µm cellulose acetate membrane filter and separated into two aliquots for cation and anion analyses. Some solutions were generated by merging several crush-leach solutions of about 15 g of fluorite crystals from the same sample to increase ion concentration (ESM1, Tables S4 and S5). Thirty-five samples were prepared from Pierre-Perthuis and thirty-two from La Collancelle (ESM1, Table S6).

The cation composition (Na, K) of fourteen samples from Pierre-Perthuis was measured using an atomic absorption spectrometer – AAS (240 FS Varian) in fast sequential mode at Géosciences Paris-Saclay (GEOPS). Thirteen other samples from Pierre-Perthuis and thirty-two from La Collancelle were analyzed using ion chromatography using a Dionex Aquion ion chromatography system with a Dionex IonPac CS-16 column and IonPac CG-16 guard column (Thermo Fischer Scientific, Waltham, USA) at GEOPS. These aliquots were acidified with 0.2 mL of ultrapure HNO_3^- (AnalaR NORMAPUR®, down to pH=2) triply distilled using the DST 1000 Savillex system to minimize adsorption and reprecipitation of calcium (Gleeson et al. 2003, Köhler et al. 2009). The second aliquot from these samples were used to quantify the anions (Cl, Br) by ion chromatography using an ICS-1000 Dionex with a Dionex IonPac AS-14 column and IonPac AG-14 guard column at GEOPS.

Thirteen electrolytic solutions generated from Pierre-Perthuis samples and eighteen from La Collancelle samples were analyzed at the BRGM by ion chromatography using a Dionex Aquion system (Thermo Fischer Scientific, Waltham, USA) for chlorine concentration and by ICP-MS for bromine and lithium concentrations (Table S6).

Uncertainties on the anion and cation concentrations were determined by repeated measurements of standard solutions and are given with a 95% confidence interval. Concentrations of fluid inclusions have been recalculated by applying a correction factor obtained by comparing the chlorine concentration obtained by crush-leach analyses and the mean of those calculated by microthermometry. These correction factors have been applied to all elements measured by crush-leach solutions (Banks et al. 2000). The major cation and anion content in the fluid inclusion leachates is expressed in ppm of solution and is discussed in the text in terms of molar ratios.

Fluid inclusion chlorine stable isotope composition

For each sample, 90 to 120 g of fluorite crystals were extracted and prepared following the dissolved ion crush-leach. Five samples were analyzed from Pierre-Perthuis and three from La Collancelle. Unfractionated chloromethane of sufficient purity for isotope measurements was produced in three steps: (1) precipitation of silver chloride by addition of silver nitrate ($AgNO_3$), (2) reaction of silver chloride with iodomethane (CH_3I) and (3) separation by gas chromatography. $\delta^{37}Cl$ was then measured on a dual-inlet gas source mass-spectrometer Finnigan Delta plus XP (Thermo Fisher Scientific) at the Institut de physique du globe de Paris (IPGP, Université Paris Cité) on gaseous CH_3Cl. The overall analytical procedure follows the methods developed by Kaufmann et al. (1984), detailed by Eggenkamp (1994). Data is reported in per mil variations relative to Standard Mean Ocean Chlorine (SMOC, Godon et al. 2004). The external reproducibility for the internal seawater standard was ±0.031 ‰ (1σ, n =4) for the first session and ±0.005 ‰ (1σ, n =3) for the second (ESM1).

Results

Data significance

The significance of the fluid inclusions leachate analyses is examined by considering the (1) origin of fluid inclusions, (2) potential contamination of the solutions and (3) analytical bias.

(1) Origin of fluid inclusions

Crystals selected for this research are homogenous under cathodoluminescence microscopy (Fig. 2f). Most of the fluid inclusion assemblages were interpreted as primary or pseudo-secondary (Goldstein and Reynolds 1994). However, the occurrence of secondary inclusions in our samples could not be excluded, since a significant proportion of fluid inclusions could not be unambiguously attributed to well-defined fluid inclusion assemblage. Some liquid-only aqueous inclusions were observed (Fig. 3c), interpreted here as in a metastable state (Roedder 1984; Diamond 2003). The proportion of these single-phased fluid inclusions was estimated to be less than 5% of the total fluid inclusions content. These single-phased fluid inclusions were assumed to have the same composition as the primary fluid inclusions.

Finally, a large portion of fluid inclusions appeared to be opened and leaked in both deposits, not affecting the leachate composition.

(2) Potential contamination

A series of tests was conducted to evaluate potential sources of contamination of the solutions generated by the bulk crush-leach of fluorite crystals (Fig. 12 in Appendix, Table S5 in ESM1). Elemental ratio values (Cl/Br, Na/Br, Na/K) are comparable from one leachate to another. Based on these results and the repeated analysis of blank solutions during the crush-leach analysis (ESM1, Table S4), we conclude that there is minimal contamination in Cl, Br, Na and K in our solutions.

(3) Analytical bias

Because Br content was less than 1 mg/L in almost all crush-leach solutions, two quantification methods were employed: ion chromatography (Br detection limit =50 µg/L) and ICP-MS (Br detection limit =10 µg/L), yielding

comparable values (ESM1 Tables S6 and S7). Hence, we conclude that there is no significant analytical bias, and that the Cl/Br and Na/Br ratios accurately represent those of the fluorite-mineralizing fluids.

Fluid inclusion petrography and microthermometry

Fluid inclusions were classified depending on geometric criteria relative to the host mineral as 1) isolated inclusions assumed primary in origin, 2) inclusions aligned or distributed in clusters along planes parallel to the mineral growth zones, also assumed primary in origin, 3) pseudo-secondary fluid inclusion assemblages that are not along planes parallel to the mineral growth zones, and that do not crosscut the growth zones of the mineral or 4) secondary fluid inclusion planes crosscutting mineral growth zones.

Complex fluid inclusion assemblages coexist in both deposits (Fig. 3a). In all samples, fluid inclusions are aqueous and contain mostly two phases (H_2O liquid and vapor). Most of the very large fluid inclusions (>50 µm) decrepitated and form clusters located along growth bands or cleavages (Fig. 3a, b).

The fluid inclusions in fluorite of Pierre-Perthuis are of two-types, either isolated and large (>20 µm; Fig. 3.d) or small (<20 µm) and in growth zones (Fig. 3f). In fluorite samples from La Collancelle, fluid inclusions appear as (1) primary, isolated, elongated and large (10 µm < FI size <40 µm) (Fig. 3e), (2) aligned along planes that do not intersect the mineral growth zones (Fig. 3f) and (3) randomly distributed in clusters according to the growth planes (>40 µm) (Fig. 3a, g).

Rare and small monophasic liquid inclusions (<10 µm) are observed either as metastable fluid inclusion in a plane of two-phase aqueous fluid inclusions or aligned along planes at the growth zones of crystals. The latter are considered negligible in comparison to the total volume of fluid inclusions (estimated <5%, Fig. 3h).

Some two-phase fluid inclusions (isolated or aligned along planes) cannot be assigned to a well-defined fluid inclusion assemblage. If the liquid/vapor ratio is the same as in primary fluid inclusions, these two-phase fluid inclusions were assumed to be of primary origin.

Evidence of post-trapping deformation and necking-down were observed in some primary fluid inclusion assemblages, showing variable L/V ratios. These fluid inclusions with inconsistent L/V ratios represent less than 5% of the inclusions in each fluid inclusion assemblage. These fluid inclusions were excluded for microthermometric measurements. Secondary fluid inclusion planes crosscutting mineral growth zones were not observed.

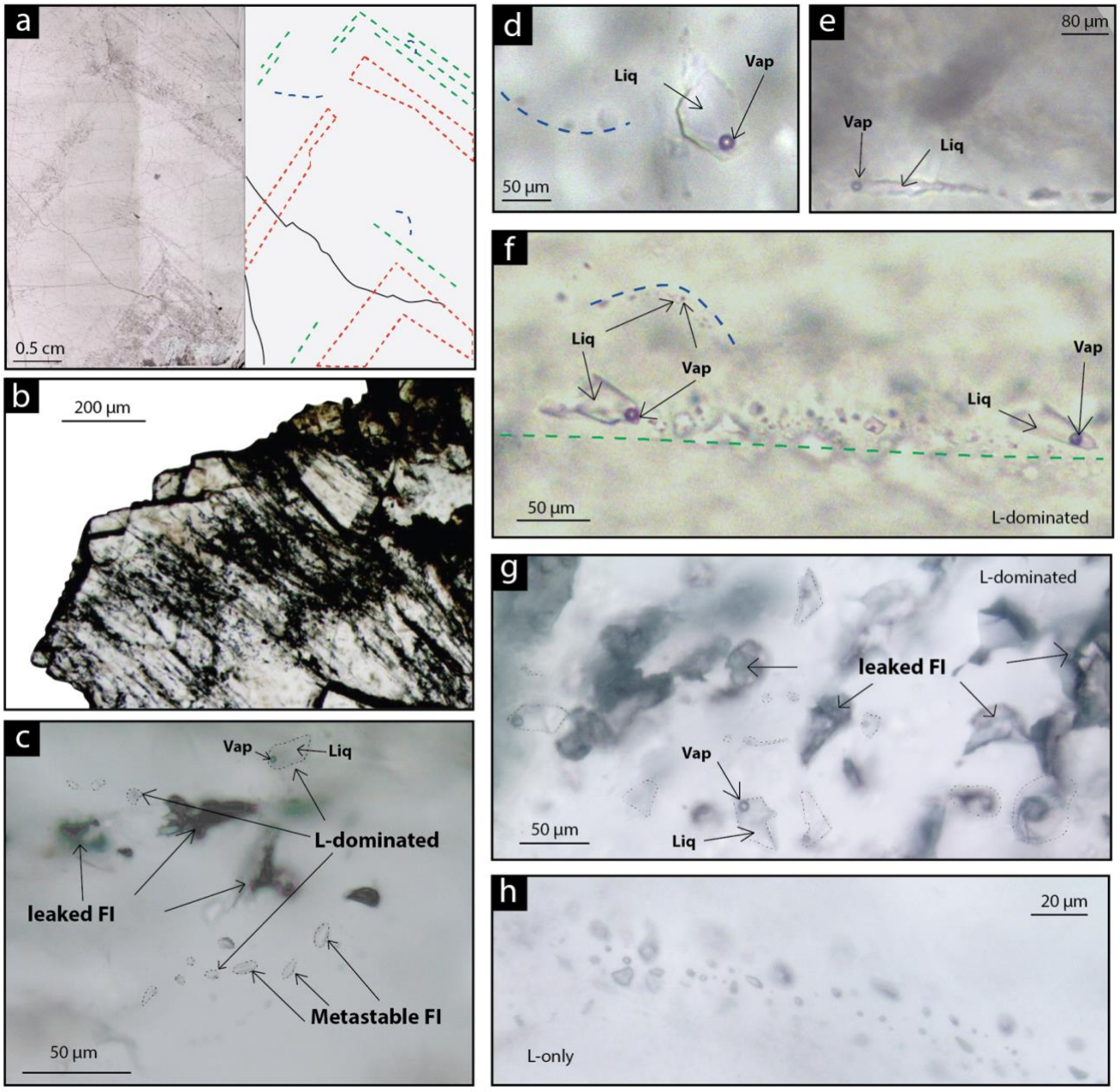

Fig. 3 Fluorite fluid inclusion petrography. (a) Schematic presentation of typical fluid inclusion assemblages in fluorite from La Collancelle. (b) Clusters of large opened and leaked inclusions along sub-parallel fractures in a fluorite crystal from Pierre-Perthuis. (c) Complex fluid inclusion assemblage in fluorite samples example from Pierre-Perthuis. (d) and (e) Isolated fluid inclusion interpreted as primary from Pierre-Perthuis. Blue dashed line indicates a pseudo-secondary

plane. (f) Fluid inclusion assemblage of liquid-vapor aqueous inclusions aligned along a growth zone represented by the green dashed line from La Collancelle. (g) Cluster of fluid inclusions from La Collancelle, that includes leaked, one-phase and two-phases inclusions. (h) Fluid inclusion plane containing single-phased aqueous-liquid inclusions from Pierre-Perthuis

Fluorite crystals in both deposits contain abundant fluid inclusions that are almost devoid of solid inclusions, except for some rare and small co-precipitated hematite that does not significantly contribute to the bulk fluid characterization. Homogenization temperatures (Th) vary from 80 to 245 °C with 85% of the measurements between 80 and 110 °C at Pierre-Perthuis and from 67 to 231 °C with more than 75% of the values between 80 and 120 °C at La Collancelle (Fig. 4a). The primary and pseudo-secondary fluid inclusions in each deposit yield the same range of Th values.

In both fluorite deposits, the first apparent melting (Te*) occurred at –48 °C ± 5 (2 σ) consistent with the eutectic of the H_2O-NaCl-$CaCl_2$ system (Yanatieva 1946, Steele McInnis et al. 2011). Hydrohalite systematically dissolved before ice. Hydrohalite final dissolution temperatures range from −48 to −25 °C and from −36 to –21 °C at Pierre-Perthuis and La Collancelle, respectively. Ice melting temperatures were between –14 and –1 °C at Pierre-Perthuis and from −16 to 0 °C at La Collancelle. Total salinity (NaCl + $CaCl_2$) thus varies from 13 to 21 wt% in Pierre-Perthuis and from 0 to 19 wt% in La Collancelle. Fluid inclusions from Pierre-Perthuis have on average a higher total salinity than those of La Collancelle (14 vs. 11 wt%) and are more calcic (with average of 12.8 and 6.8 wt% $CaCl_2$= at Pierre-Perthuis and La Collancelle, respectively). Na/Ca ratios are highly variable, with a median value of 0.2 at Pierre-Perthuis (n=67) and 0.7 at La Collancelle (n=24). Microthermometry data are summarized in Table 1 and reported in ESM1, Table S2. The composition of fluid inclusion is plotted in a NaCl-$CaCl_2$-H_2O ternary diagram in Fig. 4b.

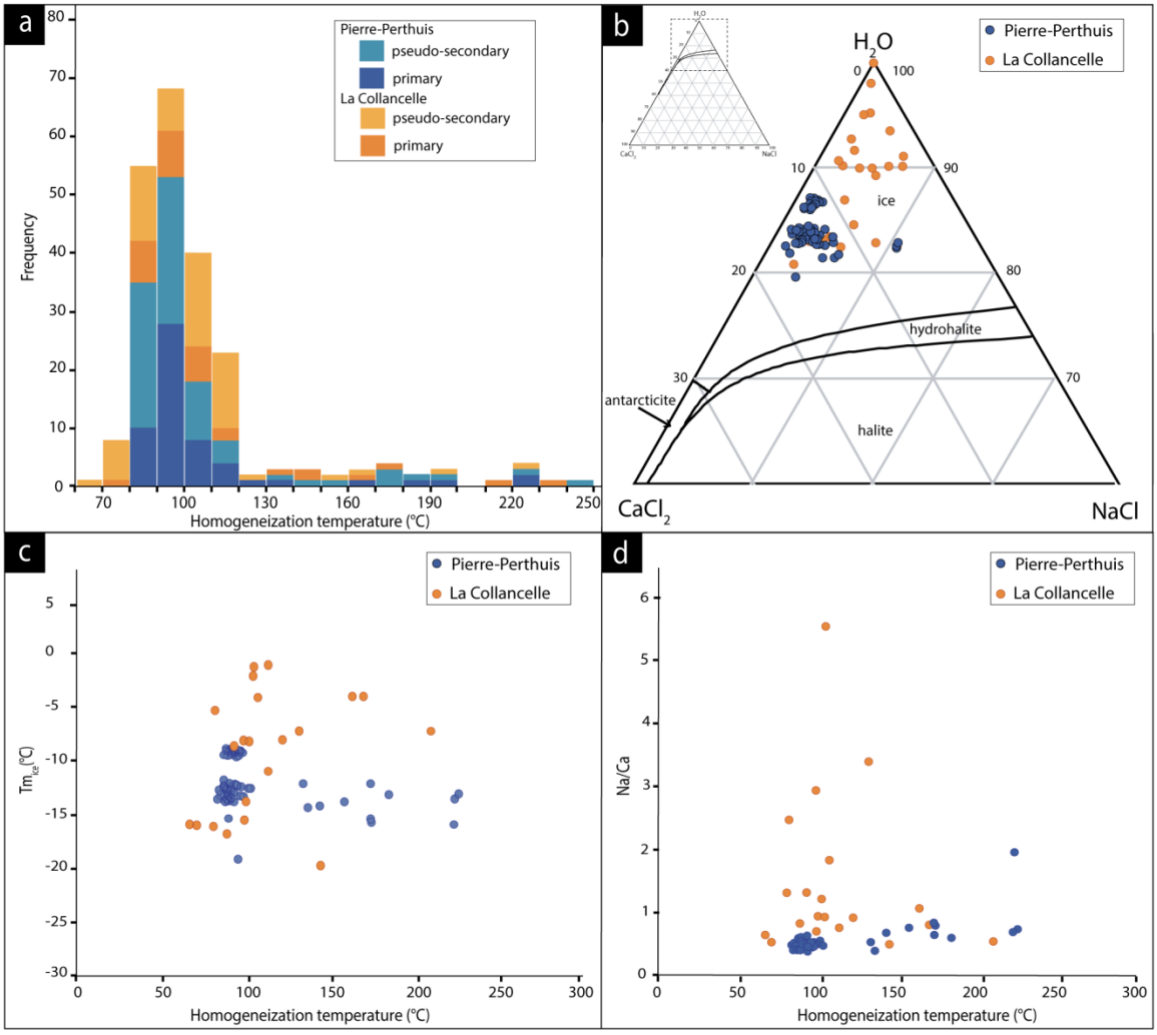

310

311 **Fig. 4** (a) Histogram of homogenization temperature (Th) according to the type of fluid inclusions, (b) Fluid inclusion

312 composition in the H_2O-NaCl-$CaCl_2$ system, (c) homogenization temperature (Th) as a function of ice melting

313 temperature (Tm_{ice}), (d) Na/Ca vs. Th.

314

315

316

317

fluorite deposit	type of fluid inclusion	Th				Tmice				Tmhh				Te*				Swt				wt% NaCl				wt% $CaCl_2$			
		min	max	med	n	min	max	med	n	min	max	med	n	min	max	med	n	min	max	med	n	min	max	med	n	min	max	med	n
Pierre-Perthuis	primary	+84	+181	+97	#	–19.3	–12.0	–14,4	9	–37.9	–34.4	–37,3	6	–50	–45	–48	4	16	21	17	6	1,4	3,7	2	6	##	16,8	12,9	6
	pseudo-secondary	+85	+136	+100	#	–15.4	–14.1	–14.4	4	–44.6	–24.7	–32.1	3	-	-	-	0	18	18	18	3	1,4	10,7	6	3	7	16	11,5	3
	All fluid inclusion	+84	+181	+97	#	–19.3	–12.0	–14,4	#	–44.6	–24.7	–36.7	9	–50	–45	–48	4	16	21	18	9	1,4	10,7	2	9	7	16,8	14,6	9
La Collancelle	primary	+74	+231	+99	#	–17.4	0	–3.9	#	–36.0	–20.9	–26.8	#	–50	–43	–48	#	0	19	9,6	9	0	10,7	3	9	0	16	5,4	9
	pseudo-secondary	+67	+223	+101	#	–16.4	–1.1	–6.5	#	–34.3	–20.9	–28.6	#	–54	–43	–49	#	2	18	10	#	0,9	7,4	4	#	1	14	6,4	15
	All fluid inclusion	+67	+231	+101	#	–17.4	0	–6.2	#	–36.0	–20.9	–28.1	#	–54	–43	–48	#	0	19	10	#	0	10,7	4	#	0	16	6,2	24

Table 1 Summary of microthermometric data for fluid inclusions from Pierre-Perthuis and La Collancelle, according to the type of fluid inclusions

Oxygen, hydrogen and chlorine stable isotope composition of inclusion fluids

The $\delta^{18}O$ of inclusion water at Pierre-Perthuis varies from –7.8 to –5.0 ‰ whereas δD ranges from –51.2 to –37.0 ‰. La Collancelle fluorite samples yield $\delta^{18}O$ values between –7.8 and –4.2 ‰, while the δD values are between –40.1 and –23.2 ‰ (Table 2).

Locality	Sample		$\delta^{18}O$ (‰$_{V\text{-}SMOW}$)	δD (‰$_{V\text{-}SMOW}$)	$\delta^{37}Cl$ (‰SMOC)
Pierre-Perthuis	PP16	min	–7.8	–51.2	−2.19
		max	–5.0	–37.0	−1.88
		med	–5.9	–40.5	−2.04
		n	7	7	2
	PP19-3	n=1	–7.9	–51.2	-
	PP14	n=1	-	-	−1.76
	PPFl	min	-	-	–2.10
		max	-	-	–2.07
		med	-	-	–2.09
		n	-	-	2
La Collancelle	COL19	min	–7.8	–38.9	–1.95
		max	–4.2	–27.1	–1.31
		med	–5.8	–33.8	–1.92
		n	8	8	3

Table 2 Oxygen, hydrogen and chlorine isotopic compositions of fluid inclusions in fluorite from Pierre-Perthuis and La Collancelle deposits

329 $\delta^{37}Cl$ values of Pierre-Perthuis fluorite samples vary from −2.19 to −1.76 ‰ with an average of −2.00 ± 0.17 ‰ (Table
330 2). La Collancelle samples vary from −1.95 to −1.31 ‰ with an average of −1.73 ± 0.36 ‰ (Table 2). Both are
331 significantly depleted in ^{37}Cl relative to seawater ($\delta^{37}Cl$=0 ‰) and chlorides from evaporite minerals (−1< $\delta^{37}Cl$ ‰ <
332 0.6; Eggenkamp 1994).
333
334 **Ion composition**
335 Pierre-Perthuis and La Collancelle fluid inclusions have average Cl concentrations estimated from microthermometry
336 of 100,000 ppm (66 values) and 69,900 ppm (24 values), respectively (ESM1, Table S7). The concentrations obtained
337 from crush-leach solutions and the calculated concentrations from the average salinity obtained from
338 microthermometric measurements are reported in ESM1 (Table S7). The molar Cl/Br ratio varies from 216 to 406 at
339 Pierre-Perthuis and from 260 to 521 at La Collancelle.
340

Discussion

Origin and physical-chemical characteristics of mineralizing brines

Temperatures and salinities of fluids

Nigon (1988) documented a minimum trapping temperature for fluorite deposits from Marigny-sur-Yonne (about 20 km from Pierre-Perthuis and 10 km from La Collancelle, Fig. 1b) between 75 and 125 °C. Here, minimal trapping temperatures for both fluorite deposits range from 85 to 115 °C, in agreement with Gigoux et al. (2016). This temperature range is consistent with the stability limit of the yellow coloration in fluorite (around 250 °C, Trinkler et al. 2005). Th higher than 115 °C are mostly measured in the largest inclusions, suggesting post-trapping deformation (Fig. 11). Variations in Th and salinity measured in primary fluid inclusions have commonly been observed in similar contexts (Richard et al. 2016; Walter et al. 2017; Scheffer et al. 2019) and may have been caused by natural fluctuations in the fluid temperature, the formation depth or variable fluid mixing ratios.

The geodic fluorite of Pierre-Perthuis was dated at 130 ± 15 Ma by Sm–Nd geochronology (Gigoux et al. 2015). Barbarand et al. (2013) estimated a maximum thickness of sedimentary cover during the Early Cretaceous period of about 1.3 kilometers in the northwestern part of the Morvan Massif and therefore a maximum burial temperature of around 70 °C for Triassic rocks using a Cretaceous geothermal gradient of 40 °C/km and a mean surface temperature of 25 °C. This estimation is consistent with the host rocks temperatures of about 60-65 °C during the Early Cretaceous determined from the maturity of sedimentary organic matter (Uriarte 1997). Consequently, the mineralizing fluids were at least 10 to 40 °C warmer than the host sedimentary rocks during fluorite crystallization, considering the minimal trapping temperatures obtained from FI microthermometry from 85 to 115 °C. Assuming a hydrostatic pressure gradient and a trapping pressure of fluid inclusions approximately at 100 bars, a correction of about + 5°C should be applied to obtain the trapping temperatures (Fig. 13).

The total salinity of fluid inclusions in La Collancelle displays variations from 0 to 19 wt% that could be interpreted as a result of a mixing between two fluids: a $CaCl_2$-rich brine diluted by seawater and/or meteoric water. At Pierre-

Perthuis, the total salinity is more homogeneous, indicating either a single fluid source or fluids having been well-mixed before fluorite precipitation.

Fluid temperature was calculated using various Na/K and Na/Li geothermometers (Table 5) proposed in literature (Truesdell 1976; Fournier 1979; Tonani 1980; Arnórsson et al. 1983; Kharaka et al. 1982; Nieva and Nieva 1987; Giggenbach 1988; Verma and Santoyo 1997). These chemical geothermometers return temperatures from 150 to 250 °C, about a hundred degrees higher than the minimum trapping temperature of fluid inclusions given by the homogenization temperature. The Na/K ratios in geothermal fluids are essentially controlled by reactions with K-feldspar and albite (Arnórsson et al. 1983). At Pierre-Perthuis and La Collancelle, the feldspar reservoir is the underlying granitic basement. Consequently, the equilibrium temperatures provided by Na/K geothermometry tend to show the involvement of a basement brine that reached chemical equilibrium at a depth of about 4 to 8 km, considering a geothermal gradient of about 30 °C/km. The ascent of these solutions towards the basement-sedimentary cover unconformity would be accompanied by a temperature drop of about 100 °C. Such a difference in temperature from fluid inclusion microthermometry and the Na/K geothermometer was previously reported in fluorite veins from the Montroc and Le Burc deposits, south of the French Massif Central (Deloule 1982). In present-day deep aquifers of the Rhine graben, Na/K and Na/K/Ca geothermometers yield temperatures about 100 °C higher than measured bottom hole temperature (Pauwels et al. 1993; Aquilina et al. 1997; Sanjuan et al. 2016).

However, the temperatures provided by these chemical geothermometers may be overestimated in the case of evaporated seawater that reached halite saturation. In such a case, Na will be incorporated in halite during the evaporation stage, which will lower the Na/K and Na/Li ratios leading to overestimation of temperature.

Localities **Values**	**Fournier (1979)**	**Truesdell (1976)**	**Giggenbach (1988)**	**Tonani (1980)**	**Nieva and Nieva (1987)**	**Amorsson (1983)**	**Verma and Santoyo (1997)**	**Verma and Santoyo (1997)**	**Kharaka et al. (1982)**
Geothermometers	**Na/K**							**Na/Li**	

Pierre-Perthuis	**mean**	**197**	**166**	**213**	**196**	**185**	**174**	**162**	**306**	**282**
	min	170	131	179	159	158	141	141	280	198
	max	230	205	244	242	217	211	190	328	368
	n	31	31	31	31	31	31	31	13	16
La Collancelle	**mean**	**187**	**151**	**204**	**183**	**174**	**160**	**151**	**337**	**207**
	min	159	118	178	145	147	128	133	322	200
	max	335	349	340	407	319	344	194	360	219
	n	27	27	27	27	27	27	27	14	14

Table 5 Equilibrium temperatures from various geothermometers

Focus on the source of fluids

Yellow fluorite crystals were investigated by Bill and Calas (1978) and Bill (1982), who showed thermally unstable O_3^- molecular ions, which substituted for two nearest-neighbor F^- ions. Since no significant difference in the oxygen and hydrogen isotopic composition from different fluorite samples is documented in this study, we assume that oxygen substitution in fluorite should not bias the $\delta^{18}O$ values, which are hereafter interpreted as the oxygen isotope composition of the fluid from which it precipitated.

$\delta^{18}O$ and δD values of fluid inclusions in fluorite plot close to the global meteoric water line (GMWL) (Fig. 5, Craig 1961). It is worth noting that some values plot above the GMWL suggesting isotopic shifts related to low-temperature fluid-rock interaction at depth in the basement, similar to those reported in the present-day groundwater in the FMC granite (Kloppmann et al. 2002). Values shifted to the right of the GMWL record the interaction with host carbonate rocks.

Low δD in fluid inclusions were also measured in some fluorite deposits at the northeastern and southeastern boundaries of the FMC (Sizaret et al. 2009; Munoz et al. 1999, respectively), and were interpreted to contain a main contribution of meteoric waters, despite high salinities. In Pierre-Perthuis, considering the Early Cretaceous crystallization age (Gigoux et al. 2015), the paleo-latitude of the southern Paris Basin was about 30 ° (Thierry and Barrier 2000) and the paleo-altitude was probably low. In such a paleo-geographical situation, the Early Cretaceous meteoric water should have been much less depleted in ^{18}O and D compared to the isotopic composition of our fluid

inclusions. Furthermore, the measured isotopic composition is at odds with the high salinity of the mineralizing fluid (Fig. 4) that suggests evolved seawater, unless we consider either (1) an increase in salinity acquired solely by fluid-rock interactions in the granitic basement (Stober and Bucher 2004; Burisch et al. 2016) or (2) the dissolution of evaporite.

In samples from Pierre-Perthuis, the $\delta^{18}O$ and δD values are in the range of the present-day meteoric and shallow ground waters (Delbart 2014). Thus, a plausible explanation would be to consider the isotopic values of fluid inclusions as reflecting the presence of present-day meteoric water in fluorite. It is known that water molecules are easily adsorbed on the surface of fluorite crystals (Foucaud et al. 2018). However, adsorbed water was removed during analysis. Since fluorite crystals were not washed before mechanical crushing, we also rule out any contamination during sample preparation. It is possible that the cavities generated by the leakage of fluid inclusions in fluorite crystals (Fig. 3b, c, g) were partially filled by recent meteoric waters and may have resisted desorption as the result of the high tortuosity of the porous network. The fractures may have formed from freeze-thaw in outcrop and may have been enhanced by the presence of clusters of large fluid inclusions constituting weak areas within the crystals.

At this stage, the O and H stable isotope composition cannot be reliably used to determine the origin of mineralizing fluids. The compositions may correspond to a mixing between Early Cretaceous meteoric water and recent meteoric water. The microthermometric data from fluid inclusions from La Collancelle shows some low salinity primary fluid inclusions, and fluctuations of the total salinity in several fluid inclusions belonging to the same fluid inclusion assemblage, suggesting mixing of a saline solution with diluted waters, likely meteoric in origin. Such low-salinity fluid inclusions were, however, not found in fluorite from Pierre-Perthuis.

Finally, it is worth mentioning that all fluid inclusions in barite crystals from both Pierre-Perthuis and La Collancelle have leaked. Hence, no measurements of their oxygen and hydrogen stable isotope composition were conducted. In our

case, the entire replacement of primary fluid inclusions by more recent meteoric water in barite crystals is likely, as suspected by De Graff et al. (2019) in a similar F-Ba deposit in the Harz mountains in Germany.

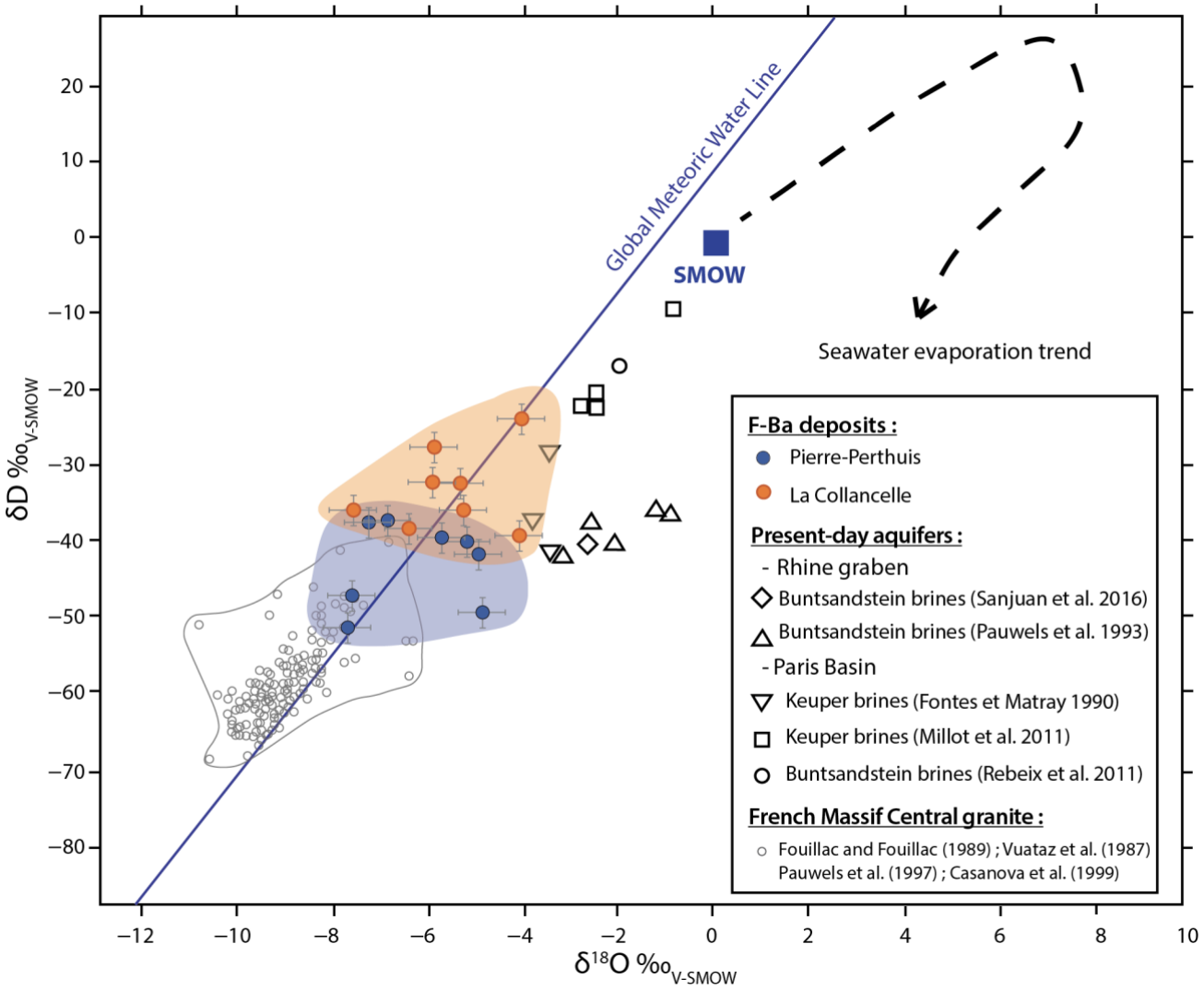

Fig. 5 Hydrogen and oxygen isotope composition of water from fluid inclusions in fluorite crystals and from contemporaneous waters in the FMC basement and in Triassic aquifers from the Paris Basin and the Rhine graben. Seawater evaporation trend is from Pierre (1982) and Global Meteoric Water Line is from Craig (1961)

Calcic-brine origin and sources of Si, F and Ba

Over the last few years, $CaCl_2$-rich brines have been detected in several fluid inclusion's studies carried on unconformity-related deposits (Lüders and Möller 1992; Banks et al. 2002; Derome et al. 2005; Gleeson and Turner 2007; Piqué et al. 2008; Richard et al. 2016; Walter et al. 2017). Moreover, $CaCl_2$-rich fluid inclusions in fluorite are common (Scheffer et al. 2019). Low Na/Ca saline solutions can be generated through several processes, including (1) dissolution of gypsum or anhydrite, (2) dissolution of calcite and dolomite or dolomitization of calcite, (3) evaporation of Cretaceous-like "$CaCl_2$ seas", (4) Na-Ca exchange reactions in silicate minerals.

(1) Dissolution of gypsum or anhydrite

The sulfate content in our fluorite fluid inclusions leachates is low (about a factor of 100 lower than Cl content). Additionally, no sulfate accumulations are known in the sedimentary rocks from the southern edge of the Paris Basin. We therefore excluded the dissolution of gypsum or anhydrite.

(2) Dissolution of calcite and dolomite or dolomitization of calcite

The first generation of fluorite in the Pierre-Perthuis deposit (Fl_{euh}, Fig. 2f) formed from the dolomitization and dissolution of the host carbonate rocks whereas the second generation, which is studied here, crystallized in cavities (Fig. 2e). Although this second fluorite generation is devoid of carbonate inclusions, it is likely that that Ca is sourced from dolomitization of the host carbonate rocks.

(3) Evaporation of Cretaceous-like "$CaCl_2$ seas"

Evaporation of Cretaceous-like seawater ("$CaCl_2$ seas") can generate brines with low Na/Ca. (Kovalevych et al. 2006; Lowenstein et al. 2001; Lowenstein and Timofeeff 2008). In the Paris Basin, the chalk deposits are of Late Cretaceous ages, i.e., post-dating the crystallization of fluorite at Pierre-Perthuis (Gigoux et al. 2015). Hence, the evaporation of Cretaceous seawater is an unlikely source of Ca.

460

461 (4) Na-Ca exchange reactions in silicate minerals

462 Albitization concomitant with the replacement of biotite by chlorite is widespread in granitic rocks of the FMC (Carrat
463 1969; Parneix et al. 1985; Cathelineau et al. 1986). In a Cl/Br vs. Na/Br plot, fluid compositions are aligned along the
464 seawater evaporation trend (Fig. 6). If Ca was mainly sourced from albitization, the Na/Br ratios of the fluids should be
465 shifted to lower values, i.e., towards the left of the seawater evaporation trend. Since such a shift is not observed in our
466 data, we conclude that Ca is not predominantly sourced from albitization processes.

467

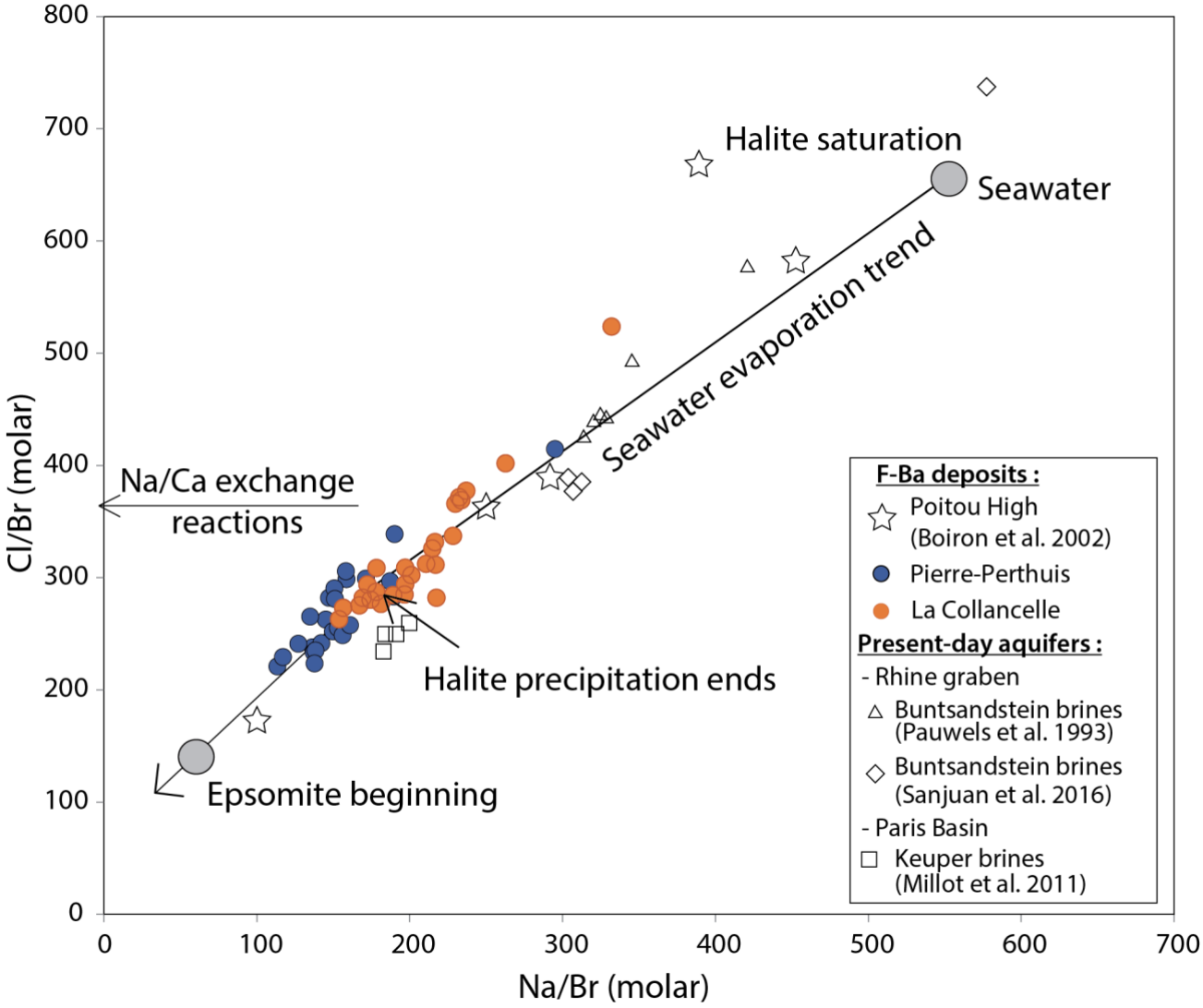

Fig. 6 Cl/Br molar ratio as a function of Na/Br molar ratio (crush-leach solutions) from fluid inclusions in fluorite from Pierre-Perthuis and La Collancelle deposits

Sources of dissolved chlorine

Cl/Br ratios measured in fluid inclusions are inconsistent with a brine derived solely from the dissolution of evaporite (Cl/Br molar ratios > 1000, Banks et al. 2000). They are also lower than the seawater value ($Cl/Br_{seawater}$ (molar) = 650, Fontes and Matray 1993; Fig. 7) but are consistent with seawater evaporation beyond halite saturation. As shown in a

476 Na/Br vs. Cl/Br plot (Fig. 6) seawater evaporation appears to be more advanced at Pierre-Perthuis than at La
477 Collancelle. Chlorine concentration in fluid inclusions is lower than seawater undergoing halite precipitation, which
478 indicates dilution by a low salinity fluid (Fig. 7; Scheffer et al. 2019). Our fluorite fluid inclusion compositions are
479 comparable with those documented by Boiron et al. (2002) in the Poitou high at the western edge of the FMC (Figs. 7
480 and 8). They are also similar to the composition of present-day brines in the Keuper (Carnian-Norian) aquifer of the
481 Paris Basin (Millot et al. 2011).
482 $\delta^{37}Cl$ values are lower than the expected value of seawater ($\delta^{37}Cl \approx 0$ ‰, Eggenkamp et al. 2019b, Fig. 8). Evaporite
483 chlorides that precipitate by evaporation of seawater have $\delta^{37}Cl$ values mostly above –0.5 ‰ (Eggenkamp et al. 2019).
484 Therefore, additional chlorine isotope fractionation processes must have occurred to produce the ^{37}Cl-depletion in
485 chlorides. This can be neither be through sequestration of ^{37}Cl in minerals because clay and other low-temperature
486 minerals contain small amounts of Cl, nor through advection which is known not to fractionate Cl^- isotopes (Bernachot
487 et al. 2017). On the other hand, slow ion transport processes, such as diffusion and ion filtration, are capable of
488 fractionating Cl^- isotopes (Desaulniers et al. 1986; Eggenkamp 1994, 2014; Agrinier et al. 2021; Strydom et al. 2022).
489 However, diffusion was shown to generate $\delta^{37}Cl$ change larger than 1 ‰ only for downstream concentrations lower
490 than 10 mM, unrealistic conditions in the aquifers of the Paris Basin, where $[Cl^-]$ is generally higher than 10 mM. Ion
491 filtration could generate ^{37}Cl-depletion of pore fluid forced through clay membranes as proposed by Agrinier et al.
492 (2019, 2021). This has been suggested as an explanation for the strong ^{37}Cl-depletion in clay-rich young sediment pore
493 fluids. It is possible that Paris Basin evaporated seawater was fractionated by ion filtration across clay-rich horizons.
494 Finally, it is worth noting that present-day deep fluids in Triassic aquifers from the central and eastern Paris Basin are
495 similarly depleted in ^{37}Cl (Fig. 8).
496

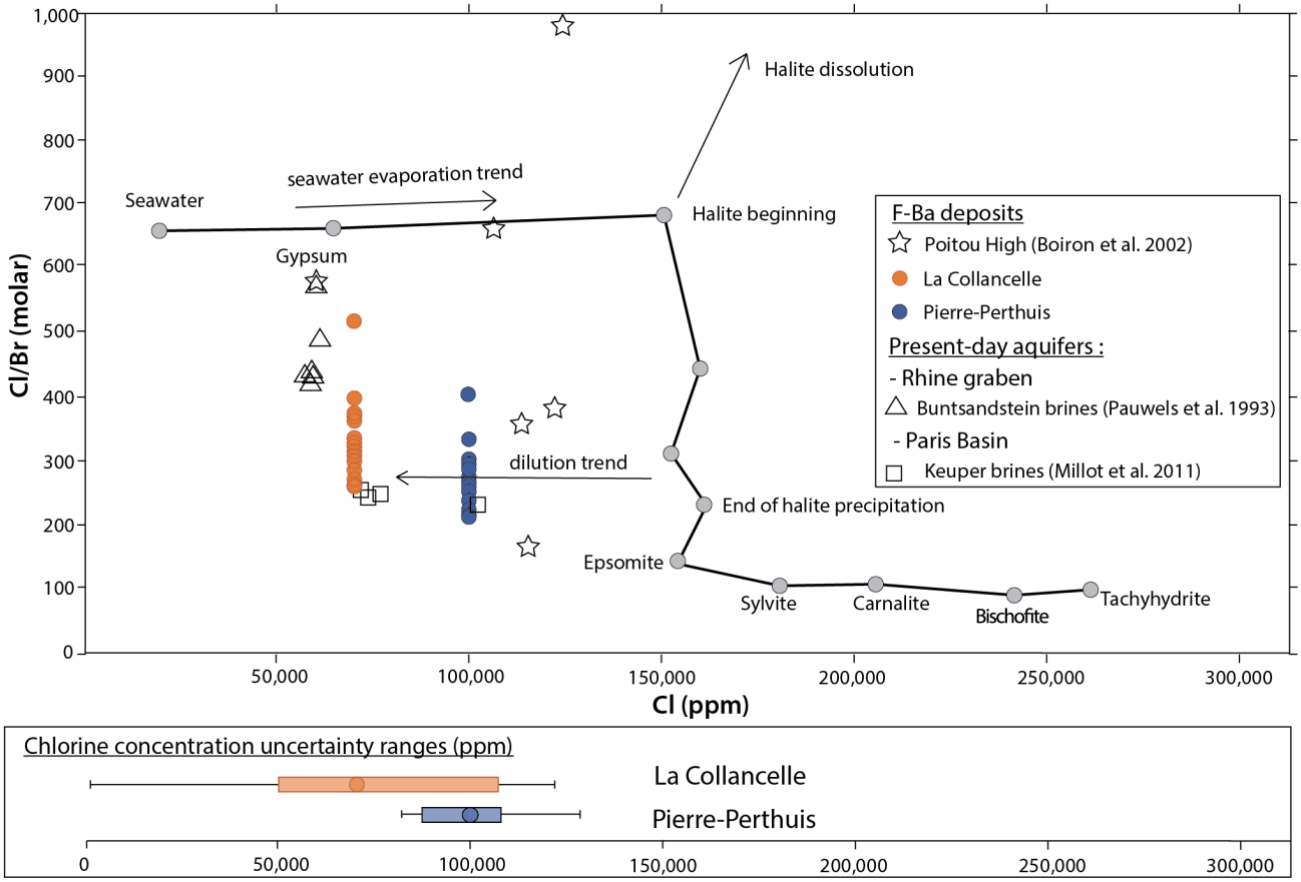

Fig. 7 Cl/Br molar ratio (crush-leach solutions) as a function of chlorine concentration (microthermometry) from fluid inclusions in fluorite from Pierre-Perthuis and La Collancelle deposits. Seawater evaporation trend according to Fontes and Matray (1993)

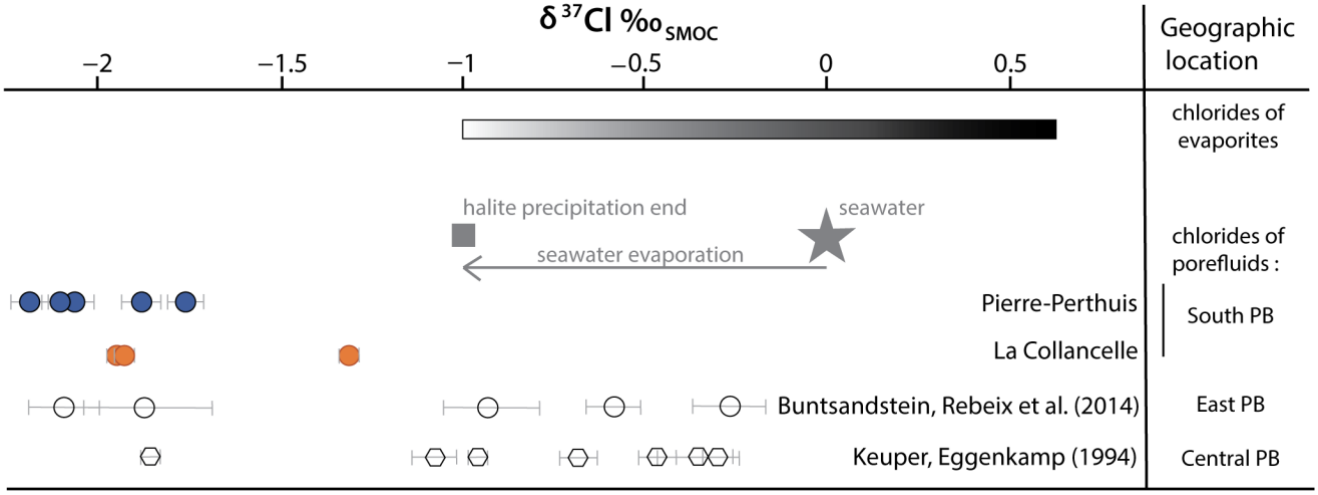

503

504 **Fig. 8** $\delta^{37}Cl$ values from fluid inclusions in fluorite from Pierre-Perthuis and La Collancelle deposits, with data from
505 the Triassic aquifers in the Paris Basin (PB). The range for chlorides in evaporite salts is from Eggenkamp et al.
506 (2019).

507

508 **Cause of fluorite precipitation**

509 Richardson and Holland (1979a) showed that the solubility of fluorite in NaCl-$CaCl_2$ solutions decreases with
510 decreasing temperature. In the Pierre-Perthuis and La Collancelle deposits, ascent of hot basement fluids through the
511 fracture network is likely, and the associated temperature decrease may have been a driving fluorite crystallization.
512 Since chlorine concentrations in fluorite fluid inclusions are lower than the expected values for seawater evaporated
513 beyond halite saturation (Fontes and Matray 1993), dilution of the basinal calcic brine by meteoric water or seawater is
514 likely (Fig. 7). Such a mixing process might explain the variations in Th measured in fluid inclusions (Fig. 4a). At La
515 Collancelle, fluid inclusions in fluorite display a large range of salinities, likely caused by variable mixing ratios
516 between a brine and meteoric or seawater (Fig. 4b).

Hence, fluorite crystallization in Pierre-Perthuis and La Collancelle was most likely triggered by the cooling of a F-rich basement brine and its mixing with less saline pore water when the solutions reached the sedimentary rocks. The partial dolomitization of the host sedimentary rock released the Ca required for fluorite to precipitate.

Comparison with present-day pore water in the Paris Basin and the Rhine graben

Millot et al. (2011) analyzed groundwater in the Keuper argillaceous sandstones located at a depth of between 2.5 and 3 km, above the Paleozoic basement, with temperatures of approximately 90 °C and chlorine concentrations ranging from 72,000 to 102,000 mg/L, comparable to those found in fluorite fluid inclusions. Matray and Fontes (1990) measured the stable isotope composition of water in the Keuper sandstones and documented values from –4 to –3 ‰ for $\delta^{18}O$ and from –40 to –25 ‰ for δD. These authors suggested that Keuper pore water originated from mixing of a sedimentary brine with meteoric waters. The nature of the brine endmember was approximated using Cl/Br ratios. Millot et al. (2011) reported molar ratios between 240 and 260. In the eastern Paris Basin, where the lower Triassic sandstones are buried at a depth of approximately 2 km, Rebeix et al. (2011) measured $\delta^{18}O$ and δD in pore water similar to the central part of the Basin, and a Cl/Br (molar) value of 167. Finally, the stable chlorine isotope composition was measured in Triassic pore waters in the eastern Paris Basin by Rebeix et al. (2014) and in the central Paris Basin by Eggenkamp (1994) who reported variable $\delta^{37}Cl$ values between –0.3 and –2.1 ‰. Hence, present-day deep Triassic fluids in the central and eastern Paris Basin display comparable chemical characteristics with paleo-fluids in Pierre-Perthuis and La Collancelle. Present-day and paleo-waters result from mixing between evaporated seawater and meteoric water. However, the main difference resides in the Na/Ca ratios of the fluids, which are much higher in Triassic aquifer water than in fluorite fluid inclusions (Fig. 9). This can be explained by the high degree of interactions with the host sedimentary rocks at Pierre-Perthuis and La Collancelle.

Basement fluids coming from a deep borehole (2.7 to 3.3 km depth) in the central Paris Basin are over-saturated with respect to CaF_2 at temperatures ranging from 100 to 120 °C (Boulègue et al. 1990). Na/Ca ratios in these basement fluids are lower than in the overlying Triassic aquifers (Fig. 9).

In the geothermal fields of the Rhine graben, the Cronenburg, Bruchsal and Bühl wells reached the Triassic and Permian reservoirs located above the granite basement, at depths ranging from about 2.5 to 2.8 km and temperatures between 115 and 140 °C (Sanjuan et al. 2016). Geothermal fluids have chlorinities ranging from 60,000 to 120,000 mg/L and Cl/Br molar ratios lower than the average seawater value (Fig. 7), which is interpreted as deriving from the evaporation of seawater (Pauwels et al. 1993). Na/Ca ratios are much higher than those measured at Pierre-Perthuis and La Collancelle, which can be explained by the shorter residence time of waters in the basement reservoir, estimated to be about 1 My (Sanjuan et al. 2016), together with a lower degree of interaction with carbonate rocks.

As a conclusion, contemporaneous waters flowing in the deep aquifers of the Paris Basin and the Rhine graben located above the crystalline basement show similar temperatures and chlorinities to the fluorite mineralizing fluids. Most of these formations waters are composed of evolved seawater diluted by meteoric water (Pauwels et al. 1993; Matray et al. 1994). The main difference resides in the Na/Ca ratios, much lower in fluorite mineralizing fluids likely as a result of dolomitization reactions.

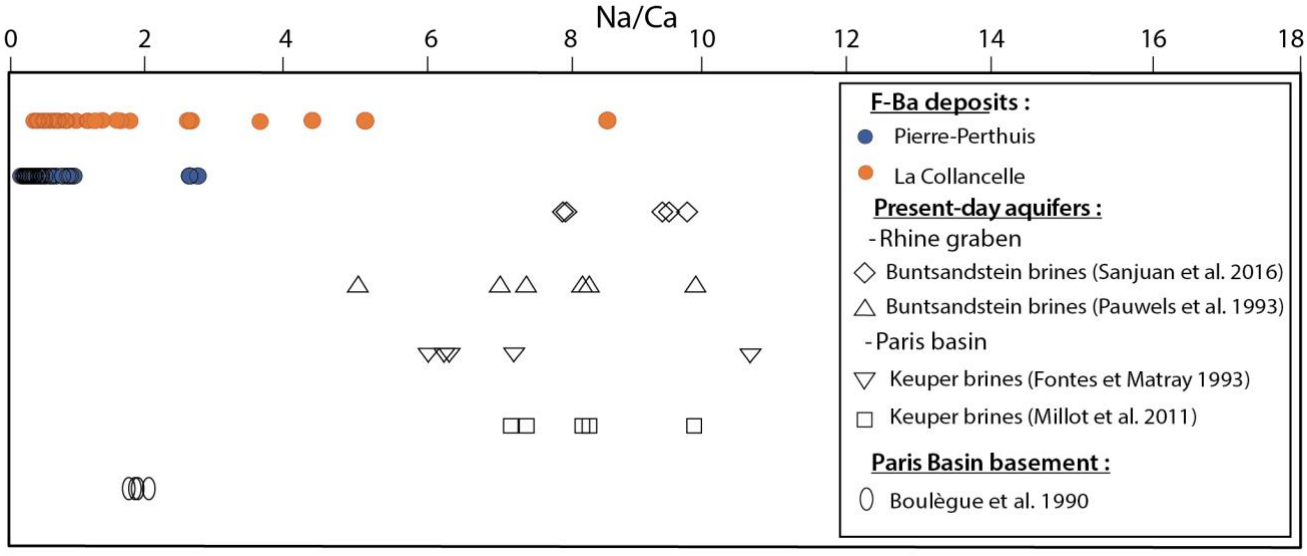

Fig. 9 Comparison of Na/Ca ratios in present-day geothermal fluids in the Paris Basin and the Rhine Graben with paleo-fluids from Pierre-Perthuis and La Collancelle fluorite deposits

557

558 **Conceptual model for F-Ba ore deposition**

559 We have shown that fluorite mineralizations in the south of the Paris Basin were formed from evaporated seawater
560 infiltrated in the basement (Fig. 7). Evaporation of seawater may have occurred at the end of the Triassic. Massive
561 halite deposits are known to exist in the basin more than 100 km north of the study area. These halite deposits are
562 broadly contemporaneous to the Assise de Chitry Formation, host of F-Ba mineralization. According to Cl/Br and
563 Na/Br ratios, the mineralizing brine passed halite saturation (Fig. 10). The evaporated seawater interacted with clay-
564 rich horizons in the basin and was depleted in ^{37}Cl through ion filtration. The dense Triassic brine penetrated
565 downward in the fractured basement and was stored in this reservoir during several tens of million years. Such long
566 residence times are conceivable for basement fluids (Fehn and Snyder 2005). We propose that this brine was diluted by
567 meteoric water and/or seawater during the Cretaceous.

568 The first fluorite mineralization event is associated with dolomitization and massive silicification of the Assise de
569 Chitry Formation, before fluorite and barite crystallization (Gigoux et al. 2016). This first generation of euhedral
570 fluorite is major in volume and formed from the dissolution and recrystallization of the host carbonate rocks (Gigoux
571 et al. 2016). The source of silica, together with the timing of silicification remains unknown. Quartz dissolution is well
572 documented in the granite of the FMC (Parneix et al. 1985; Cathelineau 1986) and constitutes a source of Si, together
573 with feldspar dissolution (Fig. 10).

574 The simultaneous chloritization of biotite and feldspar dissolution and recrystallization enriched the basement fluids in
575 F, Ba, Pb, Zn and Cu. Mineral hydration reactions may have contributed to increase the salinity of the solution (Bons
576 et al. 2014). From the Lower Jurassic to the Lower Cretaceous, continental Europe was affected by the opening of the
577 Central Atlantic and Alpine Tethys rift (Stampfli and Borel 2004; Ziegler and Dèzes 2006). The transition to the
578 Arctic-North Atlantic rift system provoked major crustal extension and subsidence in continental Europe (Burisch et
579 al. 2022) with estimation of crustal thinning of about 20 to 40 kilometers (Willner et al. 1991; Ziegler et Dèzes 2006;
580 Etheve et al. 2018). The major event of the Early Cretaceous extensional regime provoked the rifting phase in the Bay

of Biscay and caused a local compressive regime in the north of the FMC and the Paris Basin, with evidence of fault reactivation (Tremolieres 1981; Benard et al. 1985). Guillocheau et al. (2000) and De Wever et al. (2002) documented two unconformities in the sedimentary cover of the Paris Basin during the Early Cretaceous which were interpreted as a consequence of a NE–SW to E–W compression. Basement fluids were likely expelled through the reactivation of Variscan faults caused by this local compression regime (Gigoux et al. 2015). This dense Triassic brine was likely Mg-rich and may have contributed to further dolomitization and porosity generation in the surrounding sedimentary rocks. Calcium may have been sourced from the local dolomitization of the host carbonate rocks (Banks et al. 1991). Metals would have been carried in solution through chloride and/or fluoride complexes. The stability of these complexes may have drastically decreased when basement fluids mixed with less saline, S-rich solutions. Fluorite and barite, together with minor sulfides (galena, sphalerite and chalcopyrite), crystallized from (1) the temperature drop resulting from ascending fluids and (2) mixing with shallower fluids (Fig. 10). F-Ba mineralizations, associated with Pb, Zn and Cu on the southern border of the Paris Basin, are therefore comparable to other “Mississippi Valley Type” mineralizations in western Europe and northern Africa formed under the Mesozoic extensional regime (Muchez et al. 2005; Burisch et al. 2022).

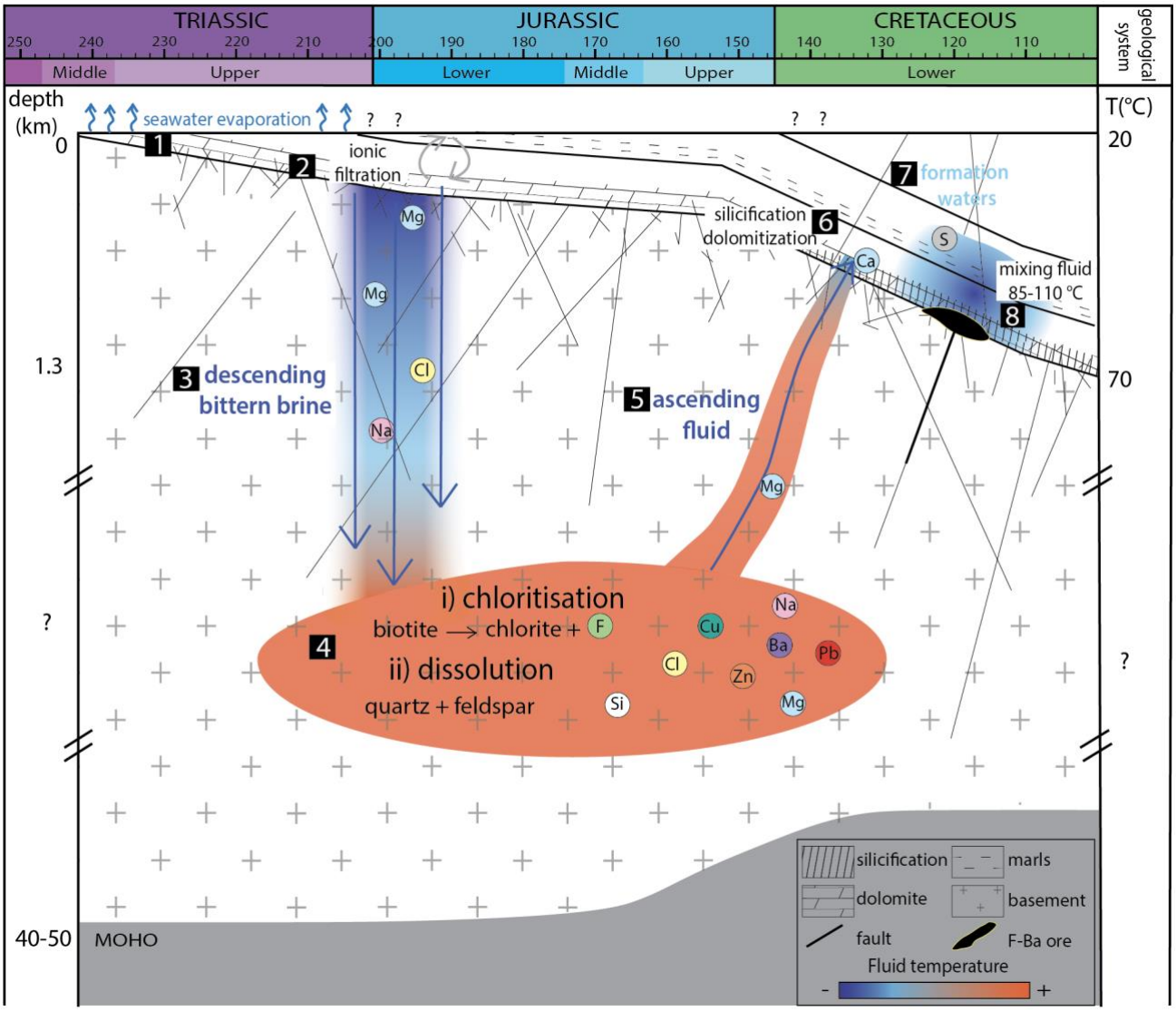

Fig. 10 Conceptual model for Early Cretaceous F-Ba deposit on the northwestern edge of the French Massif Central

Conclusion

Chemical and isotopic analysis of bulk fluid inclusions hosted in fluorite crystals from two F-Ba deposits located in the southern border of the Paris Basin provide new constraints on the origins of mineralizing fluids and the fluid-rock interactions responsible for F-Ba ores. Based on the Cl/Br ratio and chlorine concentration, evolved seawater migrated

deeply into the basement These brines were enriched in F, Ba, Pb, Zn, Cu due to biotite and feldspar dissolution and partial recrystallization, which occurred in the granitic basement. Episodic events of tectonic activity forced the brines upwards leading to ore deposition at shallower crustal levels. F-Ba mineralizations are interpreted as being the result of mixing F-Si-Cl-rich brines with SO_4-rich meteoric and/or seawater from the sedimentary basin, which decreased the solubility of fluorite. Overall, this study provides an example of granite hydrothermal alteration and fluid transfer across the crystalline basement and the overlying sedimentary reservoirs leading to unconformity-related mineralizations. The ore-forming paleofluids are analogous to present-day geothermal waters in Triassic reservoirs of the Paris Basin and the Rhine graben.

Appendix

Microthermometry

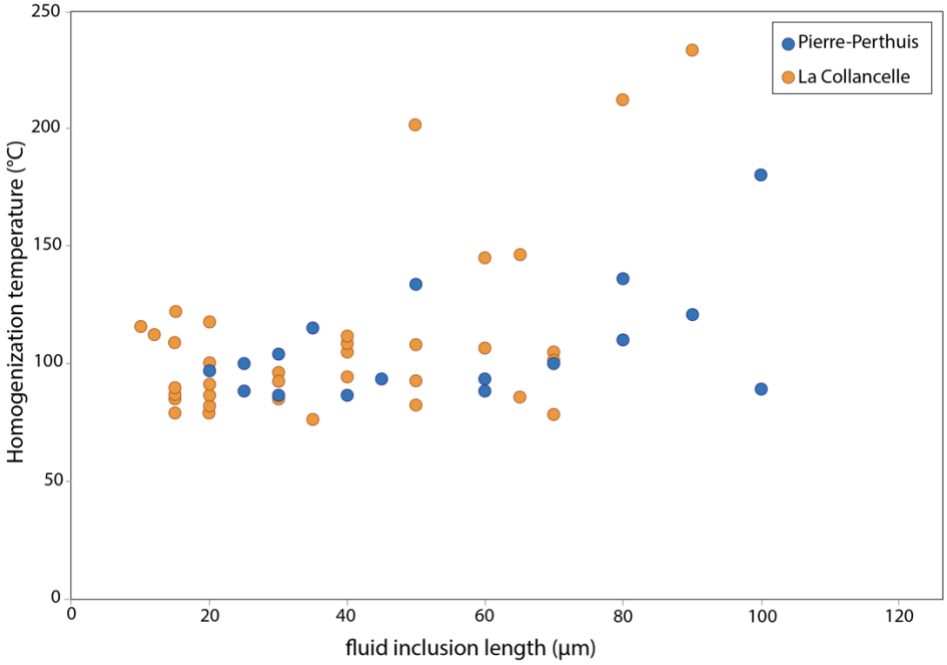

Fig. 11 Homogenization temperature vs. fluid inclusion length

Crush-leach protocol

Blank solutions were generated to test all potential sources of contamination during aliquot preparation, such as: (1) single-use equipment (plastic tubes, syringe, filter), (2) purity of MilliQ water and (3) the agate mortar. Three sets of blank solutions have been prepared and detailed in Table S4, compiled with major ions composition. Concentrations in Cl, Br, Na and K in crush-leach solutions were always at least 4 times higher, and almost always 10 times higher than in the blank solutions.

Then, we measured major dissolved ions in aliquots prepared from (1) a variable sample mass (1.5 g<m<25.4 g) and a constant volume of MilliQ water (V=10 mL; samples PP16-1 to PP16-10) and (2) a constant sample mass (m=5 g) and

a variable volume of MilliQ water (4 mL<V<20 mL; samples PP16-11 to PP16-15). Concentrations of major dissolved anions and cations from these solutions are presented in Table S5.

For a given sample mass, as the dilution volume increases, the anion concentrations decrease. In the same way, for a given dilution volume, as the sample mass increases, the anion concentrations increase.

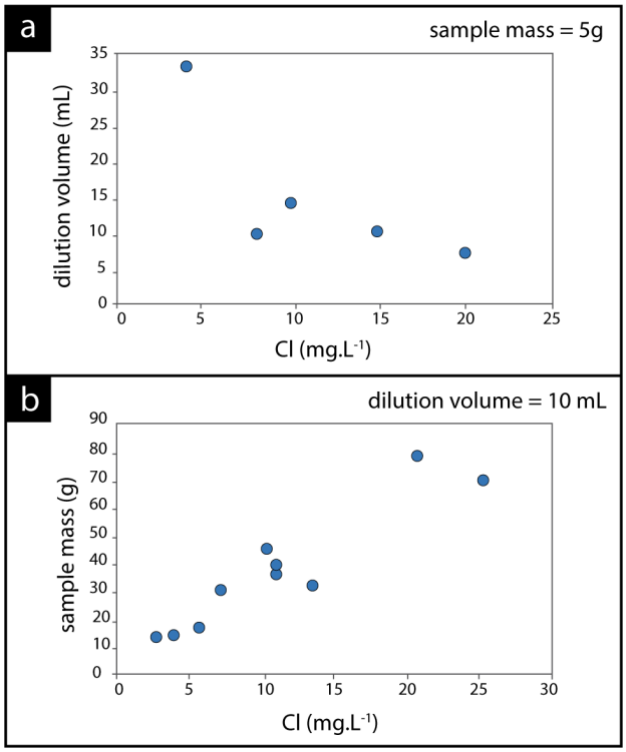

Fig. 12 Variation of chlorine concentration as a function of a) dilution volume (PP16-11 to PP16-15) for a constant mass and b) sample mass (PP16-1 to PP15-10) for a constant volume of dilution

Fluid inclusion pressure correction

Using the excel® spreadsheet from Bodnar (1993) and Steele MacInnis et al. (2012), the average slope of the dP/dT isochore is 25.1 bar/ °C at Pierre-Perthuis and 22.7 bar/ °C at La Collancelle (Fig. 13), for an average fluid density of 1.1 and 1.0 g.cm^{-3} respectively (simplified in the H_2O-NaCl system).

According to the present-day preserved sedimentary succession in the Paris Basin and Barbarand et al. (2013), the maximum sedimentary thickness during the Early Cretaceous mineralization period is about 1 km. Fluorite precipitation likely occurred under hydrostatic equilibrium at such a shallow burial depth, fluids being connected through the fracture and pore networks developed in both basement and sedimentary rocks. Considering a hydrostatic pressure gradient (Goldstein and Reynolds 1994), we therefore postulated a trapping pressure of 100 bars. Consequently, the corrected trapping temperature for fluid inclusions is around 5 degrees higher than the minimal trapping temperatures (Fig. 13).

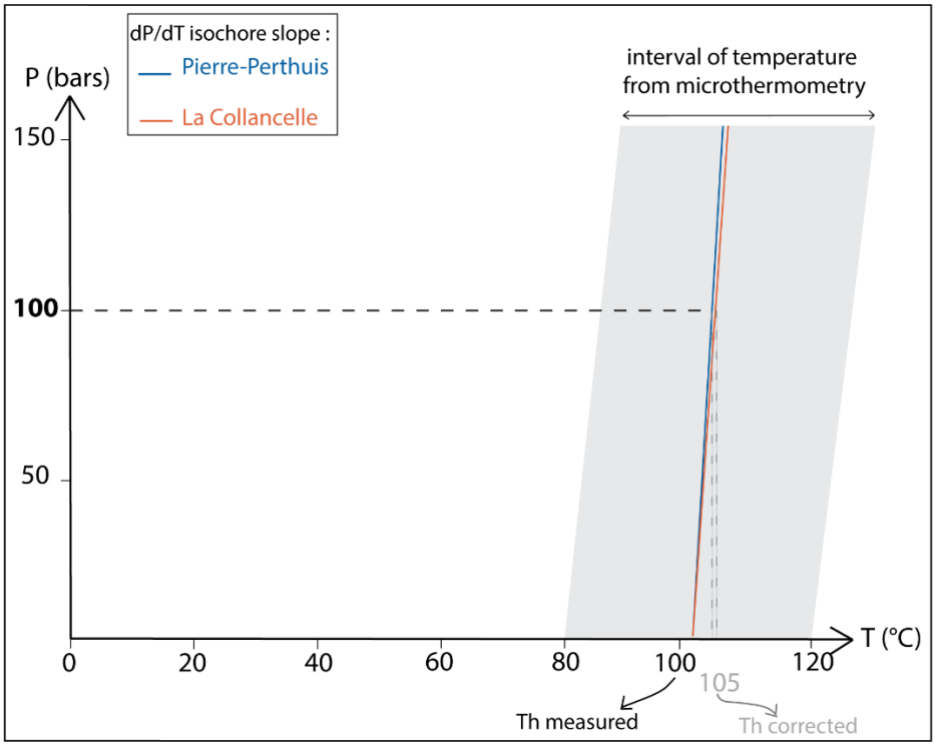

Fig. 13 P-T plots in the H_2O-NaCl system illustrating the pressure correction applied on fluid inclusions (modified after Goldstein and Reynolds 1994)

Average chlorine concentrations in fluid inclusions

The average of chlorine concentration in fluid inclusions from Pierre-Perthuis and La Collancelle has been computed from microthermometric measurements (detailed in Table 3) using the following equation:

$$Cl = \left(\frac{(wt\%NaCl \cdot 2MCl)}{MNa+MCl} + \frac{(wt\%CaCl_2 \cdot MCl)}{MCa+2MCl}\right) \cdot 1000 \qquad \text{Equation n°1}$$

With MCl=35, MNa=23 and MCa=40 (molar masses of chlorine, sodium and calcium, respectively, in $g.mol^{-1}$).

	Average of salt concentrations from microthermometry			Average Cl concentration (ppm)
Locality	Nb of value	NaCl (wt%)	$CaCl_2$ (wt%)	Cl
Pierre-Perthuis	66	3.00	12.80	100,000
La Collancelle	24	4.36	6.85	69,900

Table 3 Average chlorine concentration in ppm of fluid inclusions computed from the average of microthermometric measurements

Analytical details of Cl stable isotope composition measurements

The volume of solutions and the associated chlorinities and $\delta^{37}Cl$ of each sample is reported in Table 4.

Locality	Sample	Volume (µL)	µmol Cl/mL	δ^{37}Cl ‰$_{SMOC}$
Pierre-Perthuis	PPFl-1	17,000	0.92	−2.07
	PP14	19,800	0.61	−1.76
	PP16-1	17,500	0.44	−2.19
	PPFl-2	17,500	0.87	−2.10
	PP16-2	19,536	1.85	−1.88
La Collancelle	COL19-1	20,153	1.02	−1.92
	COL19-2	16,442	2.08	−1.31
	COL19-3	20,313	0.83	−1.95

Table 4 Summary of δ^{37}Cl (‰$_{SMOC}$) values from fluorite fluid inclusions

Statements and Declarations

Conflict of interest and funding

The authors declare that they have no conflict of interest.

Author contributions

All authors contributed to the study conception and design. Antonin Richard, Diana Chourio-Camacho and Gaël Monvoisin were involved in the crush-leach analysis. Pierre Agrinier and Gérard Bardoux supervised the quantification of stable chlorine isotopes. Thomas Rigaudier supervised the measurements of fluid inclusions oxygen and hydrogen stable isotope composition. Antonin Richard, Alexandre Tarantola, Jocelyn Barbarand and Benjamin Brigaud were involved in data interpretation and the improvement of the paper. The first draft of the manuscript was written by Louise Lenoir and Thomas Blaise and all authors read, commented on previous versions of the manuscript and approved the final version.

Acknowledgments

The authors acknowledge S. Fernando for providing crush-leach solutions of fluorite and R. Millot, S. Andrieu and T. Conte from BRGM (Bureau des Recherches Géologiques et Minières) for technical advice on ICP-MS analyses. This work was supported by the Paris Ile-de-France Region – DIM "Matériaux anciens et patrimoniaux". We would like to thank Mathias Burisch and an anonymous reviewer for the constructive comments on our manuscript, as well as associate editor David Banks and editor Georges Beaudoin.

References

Agrinier, P., Bonifacie, M., Bardoux, G., Lucazeau, F., Giunta, T., and Ader, M., 2021, Chlorine isotope data of chlorides challenge the pore fluid paradigm: Geochimica et Cosmochimica Acta, v. 300, p. 258–278, doi:10.1016/j.gca.2021.02.034.

Agrinier, P., Destrigneville, C., Giunta, T., Bonifacie, M., Bardoux, G., Andre, J., and Lucazeau, F., 2019, Strong impact of ion filtration on the isotopic composition of chlorine in young clay-rich oceanic sediment pore fluids: Geochimica et Cosmochimica Acta, v. 245, p. 525–541, doi:10.1016/j.gca.2018.11.013.

Aquilina, L., Pauwels, H., Genter, A., and Fouillac, C., 1997, Water-rock interaction processes in the Triassic sandstone and the granitic basement of the Rhine Graben: Geochemical investigation of a geothermal reservoir: Geochimica et Cosmochimica Acta, v. 61, p. 4281–4295, doi:10.1016/S0016-7037(97)00243-3.

Arnórsson, S., Gunnlaugsson, E., and Svavarsson, H., 1983, The chemistry of geothermal waters in Iceland. III. Chemical geothermometry in geothermal investigations: Geochimica et Cosmochimica Acta, v. 47, p. 567–577, doi:10.1016/0016-7037(83)90278-8.

Baatartsogt, B., Schwinn, G., Wagner, T., Taubald, H., Beitter, T., and Markl, G., 2007, Contrasting paleofluid systems in the continental basement: a fluid inclusion and stable isotope study of hydrothermal vein mineralization, Schwarzwald district, Germany: Geofluids, v. 7, p. 123–147, doi:10.1111/j.1468-8123.2007.00169.x.

Banks, D.A., Boyce, A.J., and Samson, I.M., 2002, Constraints on the Origins of Fluids Forming Irish Zn-Pb-Ba Deposits: Evidence from the Composition of Fluid Inclusions: Economic Geology, v. 3, p. 471–480, doi:doi.org/10.2113/gsecongeo.97.3.471.

Banks, D.A., Davies, G.R., Yardley, B.W.D., McCaig, A.M., and Grant, N.T., 1991, The chemistry of brines from an Alpine thrust system in the Central Pyrenees: an application of fluid inclusion analysis to the study of fluid behaviour in orogenesis: Geochemica and Cosmochemica Acta, v. 55, p. 1021–1030.

Banks, D.A., Giuliani, G., Yardley, B.W.D., and Cheilletz, A., 2000, Emerald mineralisation in Colombia: fluid chemistry and the role of brine mixing: Mineralium Deposita, v. 35, p. 699–713, doi:10.1007/s001260050273.

Barbarand, J., Quesnel, F., and Pagel, M., 2013, Lower Paleogene denudation of Upper Cretaceous cover of the Morvan Massif and southeastern Paris Basin (France) revealed by AFT thermochronology and constrained by stratigraphy and paleosurfaces: Tectonophysics, v. 608, p. 1310–1327, doi:10.1016/j.tecto.2013.06.011.

Benard, F., De Charpal, O., Mascle, A., and Tremolieres, P., 1985, Mise en évidence d'une phase de serrage Est-Ouest au Crétacé inférieur en Europe de l'Ouest : Comptes-rendus des séances de l'Académie des sciences. Série 2, Mécanique-physique, chimie, sciences de l'univers, sciences de la terre, v. 300, p. 765–768.

Bernachot, I., Garcia, B., Ader, M., Peysson, Y., Rosenberg, E., Bardoux, G., and Agrinier, P., 2017, Solute transport in porous media during drying: The chlorine isotopes point of view: Chemical Geology, v. 466, p. 102–115, doi:10.1016/j.chemgeo.2017.05.024.

Bill, H., 1982, Origin of the coloration of yellow fluorites: The O3− center structure and dynamical aspects: The Journal of Chemical Physics, v. 76, p. 219–224, doi:10.1063/1.442761.

Bill, H., and Calas, G., 1978, Color centers, associated rare-earth ions and the origin of coloration in natural fluorites: Physics and Chemistry of Minerals, v. 3, p. 117–131, doi:10.1007/BF00308116.

Bodnar, R.J., 1993, Revised equation and table for determining the freezing point depression of H2O-Nacl solutions: Geochimica et Cosmochimica Acta, v. 57, p. 683–684, doi:10.1016/0016-7037(93)90378-A.

727 Boirat, J.M., Touray, J.C., and Soulé de Lafont, D., 1980, Nouvelles observations sur le gisement stratiforme de
728 fluorine et barytine de Courcelles-Fremoy (Morvan, France): Comptes Rendus de l'Académie des Sciences, v.
729 D, p. 5–8.
730 Boiron, M.C., Cathelineau, M., Banks, D.A., Buschaert, S., Fourcade, S., Coulibaly, Y., Michelot, J.L., and Boyce, A.,
731 2002, Fluid transfers at a basement/cover interface Part II. Large-scale introduction of chlorine into the
732 basement by Mesozoic basinal brines: Chemical Geology, v. 192, p. 121–140, doi:10.1016/S0009-
733 2541(02)00191-2.
734 Boiron, M.-C., Cathelineau, M., and Richard, A., 2010, Fluid flows and metal deposition near basement /cover
735 unconformity: lessons and analogies from Pb-Zn-F-Ba systems for the understanding of Proterozoic U
736 deposits: Geofluids, doi:10.1111/j.1468-8123.2010.00289.x.
737 Bois, M., 1978, La base de la transgression mésozoïque sur la bordure ouest et nord du Morvan [Thèse de doctorat]:
738 Université de Dijon, 258, 2 vol. p.
739 Boulègue, J., Benedetti, M., Gauthier, B., and Bosch, B., 1990, Les fluides dans le socle du sondage GPF Sancerre-
740 Couy: Bulletin de la Société Géologique de France, v. 8, p. 789–795, doi:10.2113/gssgfbull.VI.5.789.
741 Brigaud, B., Bonifacie, M., Pagel, M., Blaise, T., Calmels, D., Haurine, F., and Landrein, P., 2020, Past hot fluid flows
742 in limestones detected by Δ47–(U-Pb) and not recorded by other geothermometers: Geology, v. 48, p. 851–
743 856, doi:10.1130/G47358.1.
744 Burisch, M., Markl, G., and Gutzmer, J., 2022, Breakup with benefits - hydrothermal mineral systems related to the
745 disintegration of a supercontinent: Earth and Planetary Science Letters, v. 580, p. 117373,
746 doi:10.1016/j.epsl.2022.117373.
747 Burisch, M., Marks, M.A.W., Nowak, M., and Markl, G., 2016, The effect of temperature and cataclastic deformation
748 on the composition of upper crustal fluids — An experimental approach: Chemical Geology, v. 433, p. 24–35,
749 doi:10.1016/j.chemgeo.2016.03.031.

Burisch, M., Walter, B.F., Gerdes, A., Lanz, M., and Markl, G., 2018, Late-stage anhydrite-gypsum-siderite-dolomite-calcite assemblages record the transition from a deep to a shallow hydrothermal system in the Schwarzwald mining district, SW Germany: Geochimica et Cosmochimica Acta, v. 223, p. 259–278, doi:10.1016/j.gca.2017.12.002.

Burisch, M., Walter, B.F., and Markl, G., 2017, Silicification of Hydrothermal Gangue Minerals In Pb-Zn-Cu-Fluorite-Quartz-Baryte Veins: The Canadian Mineralogist, v. 55, p. 501–514, doi:10.3749/canmin.1700005.

Burnol, L., and Lhégu, J., 1957, Chitry-les-Mines (Nièvre).: BRGM Rapport d'ensemble A 1273, 194 p.

Cardellach, E., Canals, A., and Tritlla, J., 1990, Late and post-Hercynian low temperature veins in the Catalonian Coastal Ranges: Acta geologica hispanica, v. 25, p. 75–81.

Carrat, H.G., 1969, Evolution de la granitisation et du volcanisme dans le Morvan: Bulletin de la Société Géologique de France, v. S7-XI, p. 574–587, doi:10.2113/gssgfbull.S7-XI.4.574.

Casanova, J., Bodénan, F., Négrel, P., and Azaroual, M., 1999, Microbial control on the precipitation of modern ferrihydrite and carbonate deposits from the Cézallier hydrothermal springs (Massif Central, France): Sedimentary Geology, v. 126, p. 125–145.

Cathelineau, M., 1986, The hydrothermal alkali metasomatism effects on granitic rocks: quartz dissolution and related subsolidus changes: Journal of Petrology, v. 27, p. 945–965, doi:10.1093/petrology/27.4.945.

Cathelineau, M., Boiron, M.-C., Fourcade, S., Ruffet, G., Clauer, N., Belcourt, O., Coulibaly, Y., Banks, D.A., and Guillocheau, F., 2012, A major Late Jurassic fluid event at the basin/basement unconformity in western France: 40Ar/39Ar and K–Ar dating, fluid chemistry, and related geodynamic context: Chemical Geology, v. 322–323, p. 99–120, doi:10.1016/j.chemgeo.2012.06.008.

Chu, H., Chi, G., and Chou, I.-M., 2016, Freezing and melting behaviors of H2O-NaCl-CaCl2 solutions in fused silica capillaries and glass-sandwiched films: implications for fluid inclusion studies: Geofluids, v. 16, p. 518–532, doi:10.1111/gfl.12173.

Craig, H., 1961, Isotopic Variations in Meteoric Waters: Science, v. 133, p. 1702–1703, doi:10.1126/science.133.3465.1702.

Davaine, J.J., 1980, Les croûtes silico-fluorées mésozoïques du Bazois, description et modèle d'évolution.: Mémoire BRGM Mémoire du BRGM 104, 211–241 p.

De Graaf, S., Lüders, V., Banks, D.A., Sośnicka, M., Reijmer, J.J.G., Kaden, H., and Vonhof, H.B., 2019, Fluid evolution and ore deposition in the Harz Mountains revisited: isotope and crush-leach analyses of fluid inclusions: Mineralium Deposita, v. 55, p. 47–62, doi:10.1007/s00126-019-00880-w.

De Launay, L., 1913, Traité de métallogénie, gîtes minéraux et métallifères. Gisements, recherche, production et commerce des minéraux utiles et minerais, description des principales mines.: C. Béranger.

De Wever, P., Guillocheau, F., Reynaud, J.-Y., Vennin, E., Robin, C., Cornée, A., and Rouby, D., 2002, Deux siècles de stratigraphie dans le bassin de Paris: Comptes Rendus Palevol, v. 1, p. 399–414, doi:10.1016/S1631-0683(02)00071-4.

Delbart, C., 2014, Variabilité spatio-temporelle du fonctionnement d'un aquifère karstique du Dogger: suivis hydrodynamiques et géochimiques multifréquences; traitement du signal des réponses physiques et géochimiques [Thèse de doctorat]: Université Paris Sud - Paris XI, 233 p.

Deloule, E., 1982, The genesis of fluorspar hydrothermal deposits at Montroc and Le Burc, the Tarn, as deduced from fluid inclusion analysis: Economic Geology, v. 77, p. 1867–1874, doi:10.2113/gsecongeo.77.8.1867.

Derome, D., Cathelineau, M., Cuney, M., Fabre, C., and Lhomme, T., 2005, Mixing of Sodic and Calcic Brines and Uranium Deposition at McArthur River, Saskatchewan, Canada: A Raman and Laser-Induced Breakdown Spectroscopic Study of Fluid Inclusions: Economic Geology, v. 100, p. 1529–1545, doi:https://doi.org/10.2113/gsecongeo.100.8.1529.

Desaulniers, D.E., Kaufmann, R.S., Cherry, J.A., and Bentley, H.W., 1986, 37Cl-35Cl variations in a diffusion-controlled groundwater system: Geochimica et Cosmochimica Acta, v. 50, p. 1757–1764, doi:10.1016/0016-7037(86)90137-7.

797 Diamond, L.W., 2003, Systematics of H2O inclusions, *in* Fluid Inclusions : Analysis and Interpretation, Mineralogical
798 Association of Canada Short Course Series, v. 32, p. 55–78.
799 Diamond, L.W., Wanner, C., and Waber, H.N., 2018, Penetration depth of meteoric water in orogenic geothermal
800 systems: Geology, v. 46, p. 1063–1066, doi:10.1130/G45394.1.
801 Eggenkamp, H., 2014, The Geochemistry of Stable Chlorine and Bromine Isotopes: Berlin, Heidelberg, Springer
802 Berlin Heidelberg, Advances in Isotope Geochemistry, 174 p., doi:10.1007/978-3-642-28506-6.
803 Eggenkamp, H.G.M., 1994, δ^{37}Cl: the geochemistry of chlorine isotopes [Thèse de doctorat]: Faculteit
804 Aardwetenschappen, Universiteit Utrecht, 171 p.
805 Eggenkamp, H.G.M., Louvat, P., Griffioen, J., and Agrinier, P., 2019, Chlorine and bromine isotope evolution within a
806 fully developed Upper Permian natural salt sequence: Geochimica et Cosmochimica Acta, v. 245, p. 316–326,
807 doi:10.1016/j.gca.2018.11.010.
808 Etheve, N., Mohn, G., Frizon de Lamotte, D., Roca, E., Tugend, J., and Gómez-Romeu, J., 2018, Extreme Mesozoic
809 Crustal Thinning in the Eastern Iberia Margin: The Example of the Columbrets Basin (Valencia Trough):
810 Tectonics, v. 37, p. 636–662, doi:10.1002/2017TC004613.
811 Fehn, U., and Snyder, G.T., 2005, Residence times and source ages of deep crustal fluids: interpretation of 129I and
812 36Cl results from the KTB-VB drill site, Germany: Geofluids, v. 5, p. 42–51, doi:10.1111/j.1468-
813 8123.2004.00105.x.
814 Fontes, J.-C., and Matray, J.M., 1993, Geochemistry and origin of formation brines from the Paris Basin, France 1.
815 Brines associated with Triassic salts: Chemical Geology, v. 109, p. 149–175, doi:doi.org/10.1016/0009-
816 2541(93)90068-T.
817 Foucaud, Y., Badawi, M., Filippov, L.O., Filippova, I.V., and Lebègue, S., 2018, Surface properties of fluorite in
818 presence of water: An atomistic investigation: The Journal of Physical Chemistry B, v. 122, p. 6829–6836,
819 doi:10.1021/acs.jpcb.8b02717.

820 Fouillac, C., and Fouillac, A.-M., 1989, Etude chimique et isotopique des sources minérales de l'Ardèche:
821 Hydrogeology Journal, p. 229–236.
822 Fourcade, S., Michelot, J.L., Buschaert, S., Cathelineau, M., Freiberger, R., Coulibaly, Y., and Aranyossy, J.F., 2002,
823 Fluid transfers at the basement/cover interface Part I. Subsurface recycling of trace carbonate from granitoid
824 basement rocks (France): Chemical Geology, v. 192, p. 99–119, doi:10.1016/S0009-2541(02)00192-4.
825 Fournier, R.O., 1979, A revised equation for the Na/K geothermometer: Transactions of the Geothermal Resources
826 Council, v. 3, p. 221–224.
827 Frape, S.K., Fritz, P., and McNutt, R.H., 1984, Water-rock interaction and chemistry of groundwaters from the
828 Canadian Shield: Geochimica et Cosmochimica Acta, v. 48, p. 1617–1627, doi:10.1016/0016-7037(84)90331-
829 4.
830 Fusswinkel, T., Wagner, T., Wälle, M., Wenzel, T., Heinrich, C.A., and Markl, G., 2013, Fluid mixing forms
831 basement-hosted Pb-Zn deposits: Insight from metal and halogen geochemistry of individual fluid inclusions:
832 Geology, v. 41, p. 679–682, doi:10.1130/G34092.1.
833 Galindo, C., Tornos, F., Darbyshire, D.P.F., and Casquet, C., 1994, The age and origin of the barite-fluorite (Pb-Zn)
834 veins of the Sierra del Guadarrama (Spanish Central System, Spain): a radiogenic (Nd, Sr) and stable isotope
835 study: Chemical Geology, v. 112, p. 351–364, doi:10.1016/0009-2541(94)90034-5.
836 Giggenbach, W.F., 1988, Geothermal solute equilibria. Derivation of Na-K-Mg-Ca geoindicators: Geochimica et
837 Cosmochimica Acta, v. 52, p. 2749–2765, doi:10.1016/0016-7037(88)90143-3.
838 Gigoux, M., 2015, Origine des minéralisations stratiformes de fluorine de la bordure sud-est du bassin de Paris [Thèse
839 de doctorat]: Université Paris-Sud, 307 p.
840 Gigoux, M., Brigaud, B., Pagel, M., Delpech, G., Guerrot, C., Augé, T., and Négrel, P., 2016, Genetic constraints on
841 world-class carbonate- and siliciclastic-hosted stratabound fluorite deposits in Burgundy (France) inferred
842 from mineral paragenetic sequence and fluid inclusion studies: Ore Geology Reviews, v. 72, p. 940–962,
843 doi:10.1016/j.oregeorev.2015.09.013.

844 Gigoux, M., Delpech, G., Guerrot, C., Pagel, M., Augé, T., Négrel, P., and Brigaud, B., 2015, Evidence for an Early
845 Cretaceous mineralizing event above the basement/sediment unconformity in the intracratonic Paris Basin:
846 paragenetic sequence and Sm-Nd dating of the world-class Pierre-Perthuis stratabound fluorite deposit:
847 Mineralium Deposita, v. 50, p. 455–463, doi:10.1007/s00126-015-0592-1.
848 Gleeson, S.A., and Turner, W.A., 2007, Fluid inclusion constraints on the origin of the brines responsible for Pb-Zn
849 mineralization at Pine Point and coarse non-saddle and saddle dolomite formation in southern Northwest
850 Territories: Geofluids, v. 7, p. 51–68, doi:10.1111/j.1468-8123.2006.00160.x.
851 Gleeson, S.A., Yardley, B.W.D., Munz, I.A., and Boyce, A.J., 2003, Infiltration of basinal fluids into high-grade
852 basement, South Norway: sources and behaviour of waters and brines: Geofluids, v. 3, p. 33–48,
853 doi:10.1046/j.1468-8123.2003.00047.x.
854 Godon, A., Jendrzejewski, N., Eggenkamp, H.G.M., Banks, D.A., Ader, M., Coleman, M.L., and Pineau, F., 2004, A
855 cross-calibration of chlorine isotopic measurements and suitability of seawater as the international reference
856 material: Chemical Geology, v. 207, p. 1–12, doi:10.1016/j.chemgeo.2003.11.019.
857 Goldstein, R.H., and Reynolds, T.J., 1994, Systematics of fluid inclusions in diagenetic minerals: SEPM (Society for
858 Sedimentary Geology), Short Course Notes, v. 31, 213 p., doi.org/10.2110/scn.94.31.
859 Guillocheau, F. et al., 2000, Meso-Cenozoic geodynamic evolution of the Paris Basin: 3D stratigraphic constraints:
860 Geodinamica Acta, p. 58, doi:10.1080/09853111.2000.11105372.
861 Haschke, S., Gutzmer, J., Wohlgemuth-Ueberwasser, C.C., Kraemer, D., and Burisch, M., 2021, The Niederschlag
862 fluorite-(barite) deposit, Erzgebirge/Germany—a fluid inclusion and trace element study: Mineralium
863 Deposita, v. 56, p. 1071–1086, doi:10.1007/s00126-020-01035-y.
864 Kaufmann, R., Long, A., Bentley, H., and Davis, S., 1984, Natural chlorine isotope variations: Nature, v. 309, p. 338–
865 340, doi:doi.org/10.1038/309338a0.
866 Kharaka, Y.K., Lico, M.S., and Law-Leroy, M., 1982, Chemical geothermometers applied to formation waters, Gulf of
867 Mexico and California basins.: AAPG Bulletin, v. 66, p. 588.

Kishima, Noriaki., and Sakai, Hitoshi., 1980, Oxygen-18 and deuterium determination on a single water sample of a few milligrams: Analytical Chemistry, v. 52, p. 356–358, doi:10.1021/ac50052a038.

Kloppmann, W., Girard, J.-P., and Négrel, P., 2002, Exotic stable isotope compositions of saline waters and brines from the crystalline basement: Chemical Geology, v. 184, p. 49–70, doi:10.1016/S0009-2541(01)00352-7.

Köhler, J., Schönenberger, J., Upton, B., and Markl, G., 2009, Halogen and trace-element chemistry in the Gardar Province, South Greenland: Subduction-related mantle metasomatism and fluid exsolution from alkalic melts: Lithos, v. 113, p. 731–747, doi:10.1016/j.lithos.2009.07.004.

Kovalevych, V., Marshall, T., Peryt, T., Petrychenko, O., and Zhukova, S., 2006, Chemical composition of seawater in Neoproterozoic: Results of fluid inclusion study of halite from Salt Range (Pakistan) and Amadeus Basin (Australia): Precambrian Research, v. 144, p. 39–51, doi:10.1016/j.precamres.2005.10.004.

Lardeaux, J.M., Schulmann, K., Faure, M., Janoušek, V., Lexa, O., Skrzypek, E., Edel, J.B., and Štípská, P., 2014, The Moldanubian Zone in the French Massif Central, Vosges/Schwarzwald and Bohemian Massif revisited: differences and similarities: Geological Society, London, Special Publications, v. 405, p. 7–44, doi:10.1144/SP405.14.

Lefavrais-Raymond, A., Lhégu, J., Renaud, L., and Scolari, G., 1965, Contribution à l'étude géologique et métallogénique du Nivernais septentrional (Region de Chitry-les-Mines, Nièvre): Bull BRGM, v. 2, p. 1–22.

Lenoir, L., Blaise, T., Somogyi, A., Brigaud, B., Barbarand, J., Boukari, C., Nouet, J., Brézard-Oudot, A., and Pagel, M., 2021, Uranium incorporation in fluorite and exploration of U–Pb dating: Geochronology, v. 3, p. 199–227, doi:10.5194/gchron-3-199-2021.

Lowenstein, T.K., and Timofeeff, M.N., 2008, Secular variations in seawater chemistry as a control on the chemistry of basinal brines: test of the hypothesis: Geofluids, v. 8, p. 77–92, doi:10.1111/j.1468-8123.2007.00206.x.

Lowenstein, T.K., Timofeeff, M.N., Brennan, S.T., Hardie, L.A., and Demicco, R.V., 2001, Oscillations in Phanerozoic Seawater Chemistry: Evidence from Fluid Inclusions: Science, v. 294, p. 1086–1088, doi:10.1126/science.1064280.

Lüders, V., and Möller, P., 1992, Fluid evolution and ore deposition in the Harz Mountains (Germany).: European Journal of Mineralogy, p. 1053–1068.

Mangenot, X., Bonifacie, M., Gasparrini, M., Götz, A., Chaduteau, C., Ader, M., and Rouchon, V., 2017, Coupling Δ47 and fluid inclusion thermometry on carbonate cements to precisely reconstruct the temperature, salinity and δ18O of paleo-groundwater in sedimentary basins: Chemical Geology, v. 472, p. 44–57, doi:10.1016/j.chemgeo.2017.10.011.

Matray, J.-M., and Fontes, J.-C., 1990, Origin of the oil-field brines in the Paris basin: Geology, v. 18, p. 501–504, doi:10.1130/0091-7613(1990)018<0501:OOTOFB>2.3.CO;2.

Matray, J.M., Lambert, M., and Fontes, J.Ch., 1994, Stable isotope conservation and origin of saline waters from the Middle Jurassic aquifer of the Paris Basin, France: Applied Geochemistry, v. 9, p. 297–309, doi:10.1016/0883-2927(94)90040-X.

Millot, R., Guerrot, C., Innocent, C., Négrel, Ph., and Sanjuan, B., 2011, Chemical, multi-isotopic (Li–B–Sr–U–H–O) and thermal characterization of Triassic formation waters from the Paris Basin: Chemical Geology, v. 283, p. 226–241, doi:10.1016/j.chemgeo.2011.01.020.

Muchez, P., Heijlen, W., Banks, D., Blundell, D., Boni, M., and Grandia, F., 2005, 7: Extensional tectonics and the timing and formation of basin-hosted deposits in Europe: Ore Geology Reviews, v. 27, p. 241–267, doi:10.1016/j.oregeorev.2005.07.013.

Munoz, M., Boyce, A.J., Courjault-Rade, P., Fallick, A.E., and Tollon, F., 1999, Continental basinal origin of ore fluids from southwestern Massif central fluorite veins (Albigeois, France): evidence from fluid inclusion and stable isotope analyses: Applied Geochemistry, v. 14, p. 447–458, doi:10.1016/S0883-2927(98)00070-5.

Nieva, D., and Nieva, R., 1987, Developments in geothermal energy in Mexico - part twelve. A cationic geothermometer for prospecting of geothermal resources.: Heat Recovery Systems and CHP, v. 7, p. 243–258, doi:doi.org/10.1016/0890-4332(87)90138-4.

915 Nigon, P., 1988, La fluorine stratiforme de la bordure ouest du Morvan : géologie, géochimie et modélisation.:
916 Université d'Orléans, 256 p.
917 Parneix, J.C., Beaufort, D., Dudoignon, P., and Meunier, A., 1985, Biotite chloritization process in hydrothermally
918 altered granites: Chemical Geology, v. 51, p. 89–101, doi:10.1016/0009-2541(85)90089-0.
919 Pauwels, H., Fouillac, C., and Fouillac, A.-M., 1993, Chemistry and isotopes of deep geothermal saline fluids in the
920 Upper Rhine Graben: Origin of compounds and water-rock interactions: Geochimica et Cosmochimica Acta,
921 v. 57, p. 2737–2749, doi:10.1016/0016-7037(93)90387-C.
922 Pauwels, H., Fouillac, C., Goff, F., and Vuataz, F.D., 1997, The isotopic and chemical composition of CO2-rich
923 thermal waters in the Mont-Dore region (Massif-Central, France): Applied Geochemistry, v. 12, p. 411–427.
924 Pierre, C., 1982, Teneurs en isotopes stables ($\delta^{18}O$, $\delta^{2}H$, $\delta^{13}C$, $\delta^{34}S$) et conditions de génèse des évaporites marines :
925 application à quelques milieux actuels et au Messinien de la Méditerranée [Thèse de doctorat]: Université
926 Paris-Sud.
927 Piqué, À., Canals, À., Grandia, F., and Banks, D.A., 2008, Mesozoic fluorite veins in NE Spain record regional base
928 metal-rich brine circulation through basin and basement during extensional events: Chemical Geology, v. 257,
929 p. 139–152, doi:10.1016/j.chemgeo.2008.08.028.
930 Rebeix, R. et al., 2014, Chlorine transport processes through a 2000 m aquifer/aquitard system: Marine and Petroleum
931 Geology, v. 53, p. 102–116, doi:10.1016/j.marpetgeo.2013.12.013.
932 Rebeix, R., Le Gal La Salle, C., Michelot, J.-L., Verdoux, P., Noret, A., Monvoisin, G., Gianesinni, S., Lancelot, J.,
933 and Simler, R., 2011, Tracing the origin of water and solute transfers in deep groundwater from Oxfordian,
934 Dogger and Trias formations in the east of the Paris Basin – France: Physics and Chemistry of the Earth, Parts
935 A/B/C, v. 36, p. 1496–1510, doi:10.1016/j.pce.2011.07.015.
936 Richard, A., Banks, D.A., Mercadier, J., Boiron, M.-C., Cuney, M., and Cathelineau, M., 2011, An evaporated
937 seawater origin for the ore-forming brines in unconformity-related uranium deposits (Athabasca Basin,

938 Canada): Cl/Br and δ37Cl analysis of fluid inclusions: Geochimica et Cosmochimica Acta, v. 75, p. 2792–
939 2810, doi:10.1016/j.gca.2011.02.026.
940 Richard, A., Cathelineau, M., Boiron, M.-C., Mercadier, J., Banks, D.A., and Cuney, M., 2016, Metal-rich fluid
941 inclusions provide new insights into unconformity-related U deposits (Athabasca Basin and Basement,
942 Canada): Mineralium Deposita, v. 51, p. 249–270, doi:10.1007/s00126-015-0601-4.
943 Richardson, C.K., and Holland, H.D., 1979, The solubility of fluorite in hydrothermal solutions, an experimental
944 study: Geochimica et Cosmochimica Acta, v. 43, p. 1313–1325, doi:10.1016/0016-7037(79)90121-2.
945 Roedder, E., 1984, Fluid inclusions: an introduction to studies of all types of fluid inclusions, gas, liquid, or melt,
946 trapped in materials from earth and space, and their application to the understanding of geologic processes:
947 Washington, D.C., Mineralogical Society of America ; Chelsea, Mich. : Printed by BookCrafters, Inc.,
948 Reviews in mineralogy 12, 644 p.
949 Sánchez, V., Vindel, E., Martín-Crespo, T., Corbella, M., Cardellach, E., and Banks, D., 2009, Sources and
950 composition of fluids associated with fluorite deposits of Asturias (N Spain): Geofluids, v. 9, p. 338–355,
951 doi:10.1111/j.1468-8123.2009.00259.x.
952 Sanjuan, B., Millot, R., Innocent, Ch., Dezayes, Ch., Scheiber, J., and Brach, M., 2016, Major geochemical
953 characteristics of geothermal brines from the Upper Rhine Graben granitic basement with constraints on
954 temperature and circulation: Chemical Geology, v. 428, p. 27–47, doi:10.1016/j.chemgeo.2016.02.021.
955 Scheffer, C., Tarantola, A., Vanderhaeghe, O., Voudouris, P., Spry, P.G., Rigaudier, T., and Photiades, A., 2019, The
956 Lavrion Pb-Zn-Ag–Rich Vein and Breccia Detachment-Related Deposits (Greece): Involvement of
957 Evaporated Seawater and Meteoric Fluids During Postorogenic Exhumation: Economic Geology, v. 114, p.
958 1415–1442, doi:10.5382/econgeo.4670.
959 Sizaret, S., 2003, Genèse du Système Hydrothermal à Fluorine-Barytine-Fer de Chaillac, (Indre, France) [Thèse de
960 doctorat]: Université d'Orléans, 271 p.

961 Sizaret, S., Marcoux, E., Boyce, A., Jebrak, M., Stevenson, R., and Ellam, R., 2009, Isotopic (S, Sr, Sm/Nd, D, Pb)
962 evidences for multiple sources in the Early Jurassic Chaillac F-Ba ore deposit (Indre, France): Bulletin de la
963 Société Géologique de France, v. 180, p. 83–94, doi:10.2113/gssgfbull.180.2.83.
964 Sizaret, S., Marcoux, E., Jebrak, M., and Touray, J.C., 2004, The Rossignol Fluorite Vein, Chaillac, France:
965 Multiphase Hydrothermal Activity and Intravein Sedimentation: Economic Geology, v. 99, p. 1107–1122,
966 doi:10.2113/gsecongeo.99.6.1107.
967 Soulé de Lafont, D., and Lhégu, J., 1980, Les gisements stratiformes de fluorine du Morvan (sud-est du Bassin de
968 Paris, France)., *in* Paris, France, v. Fascicules sur les gisements Français 2, p. 40.
969 Stampfli, G.M., and Borel, G.D., 2004, The TRANSMED Transects in Space and Time: Constraints on the
970 Paleotectonic Evolution of the Mediterranean Domain, *in* Cavazza, W., Roure, F., Spakman, W., Stampfli,
971 G.M., and Ziegler, P.A. eds., The TRANSMED Atlas. The Mediterranean Region from Crust to Mantle:
972 Geological and Geophysical Framework of the Mediterranean and the Surrounding Areas, Berlin, Heidelberg,
973 Springer Berlin Heidelberg, p. 53–80, doi:10.1007/978-3-642-18919-7_3.
974 Steele-MacInnis, M., Bodnar, R.J., and Naden, J., 2011, Numerical model to determine the composition of H2O–
975 NaCl–CaCl2 fluid inclusions based on microthermometric and microanalytical data: Geochimica et
976 Cosmochimica Acta, v. 75, p. 21–40, doi:10.1016/j.gca.2010.10.002.
977 Steele-MacInnis, M., Ridley, J., Lecumberri-Sanchez, P., Schlegel, T.U., and Heinrich, C.A., 2016, Application of
978 low-temperature microthermometric data for interpreting multicomponent fluid inclusion compositions: Earth-
979 Science Reviews, v. 159, p. 14–35, doi:10.1016/j.earscirev.2016.04.011.
980 Stober, I., and Bucher, K., 2004, Fluid sinks within the earth's crust: Geofluids, v. 4, p. 143–151, doi:10.1111/j.1468-
981 8115.2004.00078.x.
982 Strydom, J., Sterpenich, J., Grgic, D., Richard, A., Eggenkamp, H.G.M., Agrinier, P., Louvat, P., Mosser-Ruck, R.,
983 Gaire, P., and Gaucher, E.C., 2022, Experimental study of chemical evolution and isotope fractionation of Cl

and Br in pore water expelled during strong clay compaction: Applied Geochemistry, v. 140, p. 105274, doi:10.1016/j.apgeochem.2022.105274.

Thierry, J., and Barrier, E., 2000, Late Sinemurian, middle Toarcian, middle Callovian, early Kimmeridgian, early Tithonian.: CCGM/CGMW Atlas Peri-Tethys, Paleogeographical Maps - Explanatory Notes.

Tonani, F.B., 1980, Some Remarks on the Application of Geochemical Techniques in geothermal exploration, *in* Strub, A.S. and Ungemach, P. eds., Advances in European Geothermal Research, Dordrecht, Springer Netherlands, p. 428–443, doi:10.1007/978-94-009-9059-3_38.

Tremolieres, P., 1981, Mécanismes de la déformation en zones de plate-forme: méthode et application au bassin de Paris. Deuxième partie: Revue de l'Institut Français du Pétrole, v. 36, p. 579–593.

Trinkler, M., Monecke, T., and Thomas, R., 2005, Constraints on the genesis of yellow fluorite in hydrothermal barite-fluorite veins of the Erzgebirge, Eastern Germany: Evidence from optical absorption spectroscopy, rare earth element data, and fluid inclusion investigations: The Canadian Mineralogist, v. 43, p. 883–898, doi:10.2113/gscanmin.43.3.883.

Truesdell, A.H., 1976, Geochemical techniques in exploration, summary of section III., *in* San Francisco, California, USA, Proceedings : Second United Nations Symposium on the Development and Use of Geothermal Resources, v. 1, p. 53–79.

Uriarte, J.A., 1997, Maturité thermique des sédiments de la bordure sud-est du Bassin de Paris [Thèse de doctorat]: Université de Genève, 158 p., 10.13097/archive-ouverte/unige:98446 (accessed February 2022).

Verma, S., and Santoyo, E., 1997, New improved equations for Na/L, Na/Li and SiO2 geothermometers by outlier detection and rejection: Journal of volcanology and geothermal research, v. 79, p. 9–23.

Vialette, Y., 1973, Age des granites du Massif Central: Bulletin de la Société Géologique de France, v. S7-XV, p. 260–270, doi:10.2113/gssgfbull.S7-XV.3-4.260.

1006 Vuataz, F.D., Fouillac, A.-M., Fouillac, C., Michard, G., and Brach, M., 1987, Etude isotopique et suivi géochimique
1007 des eaux des sondages de Chassole et de quelques sources minérales du Cézallier (Massif Central, France):
1008 Géologie de la France, v. 4, p. 121–131.
1009 Walter, B.F., Burisch, M., Fusswinkel, T., Marks, M.A.W., Steele-MacInnis, M., Wälle, M., Apukhtina, O.B., and
1010 Markl, G., 2018a, Multi-reservoir fluid mixing processes in rift-related hydrothermal veins, Schwarzwald,
1011 SW-Germany: Journal of Geochemical Exploration, v. 186, p. 158–186, doi:10.1016/j.gexplo.2017.12.004.
1012 Walter, B.F., Burisch, M., Marks, M.A.W., and Markl, G., 2017, Major element compositions of fluid inclusions from
1013 hydrothermal vein-type deposits record eroded sedimentary units in the Schwarzwald district, SW Germany:
1014 Mineralium Deposita, v. 52, p. 1191–1204, doi:10.1007/s00126-017-0719-7.
1015 Walter, B.F., Gerdes, A., Kleinhanns, I.C., Dunkl, I., von Eynatten, H., Kreissl, S., and Markl, G., 2018b, The
1016 connection between hydrothermal fluids, mineralization, tectonics and magmatism in a continental rift setting:
1017 Fluorite Sm-Nd and hematite and carbonates U-Pb geochronology from the Rhinegraben in SW Germany:
1018 Geochimica et Cosmochimica Acta, v. 240, p. 158–186, doi:10.1016/j.gca.2018.08.012.
1019 Willner, A.P., Massonne, H.-J., and Krohe, A., 1991, Tectono-thermal evolution of a part of a Variscan magmatic arc:
1020 The Odenwald in the Mid-German Crystalline Rise: Geologische Rundschau, v. 80, p. 369–389,
1021 doi:10.1007/BF01829372.
1022 Yanatieva, O.K., 1946, Polythermal solubilities in the systems CaCl2-MgCl2-H2O and CaCl2-NaCl-H2O: Zhurnal
1023 Prikladnoi Khimii, v. 19, p. 709–722.
1024 Ziegler, P.A., and Dèzes, P., 2006, Crustal evolution of Western and Central Europe: Geological Society, London,
1025 Memoirs, v. 32, p. 43–56, doi:10.1144/GSL.MEM.2006.032.01.03.
1026